ONLINE TRAJECTORY PLANNING FOR NONSTIFF ROBOTIC DEBURRING MACHINES BASED ON DYNAMIC MOVEMENT PRIMITIVES METHOD

A THESIS SUBMITTED TO
THE GRADUATE SCHOOL OF NATURAL AND APPLIED SCIENCES
OF
MIDDLE EAST TECHNICAL UNIVERSITY

BY

MUSAB ÇAĞRI UĞURLU

IN PARTIAL FULFILLMENT OF THE REQUIREMENTS
FOR
THE DEGREE OF MASTER OF SCIENCE
IN
MECHANICAL ENGINEERING

OCTOBER 2018

Approval of the thesis:

ONLINE TRAJECTORY PLANNING FOR NONSTIFF ROBOTIC DEBURRING MACHINES BASED ON DYNAMIC MOVEMENT PRIMITIVES METHOD

submitted by **MUSAB ÇAĞRI UĞURLU** in partial fulfillment of the requirements for the degree of **Master of Science in Mechanical Engineering Department, Middle East Technical University** by,

Prof. Dr. Halil Kalıpçılar _____
Dean, Graduate School of **Natural and Applied Sciences**

Prof. Dr. Sahir Arıkan _____
Head of Department, **Mechanical Engineering**

Assoc. Prof. Dr. Erhan İlhan Konukseven _____
Supervisor, **Mechanical Engineering Department, METU**

Assist. Prof. Dr. A. Buğra Koku _____
Co-supervisor, **Mechanical Engineering Department, METU**

Examining Committee Members:

Assist. Prof. Dr. Kıvanç Azgın
Mechanical Engineering Department, METU _____

Assoc. Prof. Dr. E. İlhan Konukseven
Mechanical Engineering Department, METU _____

Assist. Prof. Dr. A. Buğra Koku
Mechanical Engineering Department, METU _____

Assist. Prof. Dr. Ali Emre Turgut
Mechanical Engineering Department, METU _____

Assist. Prof. Dr. Andaç Töre Şamiloğlu
Mechanical Engineering Department, Başkent University _____

Date: 09.10.2018

I hereby declare that all information in this document has been obtained and presented in accordance with academic rules and ethical conduct. I also declare that, as required by these rules and conduct, I have fully cited and referenced all material and results that are not original to this work.

Name, Last Name: Musab Çağrı Uğurlu

Signature :

ABSTRACT

ONLINE TRAJECTORY PLANNING FOR NONSTIFF ROBOTIC DEBURRING MACHINES BASED ON DYNAMIC MOVEMENT PRIMITIVES METHOD

Uğurlu, Musab Çağrı
M.S., Department of Mechanical Engineering
Supervisor : Assoc. Prof. Dr. Erhan İlhan Konukseven
Co-Supervisor : Assist. Prof. Dr. A. Buğra Koku

October 2018, 63 pages

Robotic deburring has an advance of precise and repeatable machining process on specific surface profiles. However, different from traditional deburring, deburring robots require generated trajectories on a workpiece with unknown chip thickness, which is a hard task due to the low stiffness of robot arm and abrasive tool used. This study presents a method for planning the online trajectory of a deburring robot by considering tool deflection based on the motion primitives trained from offline trajectories. From offline trajectories, task-related movements of 6-DoF deburring robot and interaction forces between the tool and the known workpiece while performing the deburring process are recorded. Then, by utilizing the laser scanner, the surface of the workpiece is measured after the deburring process in order to determine the difference between the actual depth of cut of the workpiece and given set depth of cut. The remained material is mainly because of the low stiffness of the tool which creates tool deflection. Using force data as perception and remained material as action, Dynamic Movement Primitives method is modified, then trained and used to predict deflection on the tool. The linear deflection and angular deviation compensation are performed in order to make adjustments on the trajectory while performing the deburring opera-

tion online. Finally, the form error results of the robotic deburring process with DMP is compared with three other processes; Standard robotic deburring process, robotic deburring with PID control and robotic deburring with Active Disturbance Rejection control.

Keywords: Deburring Process, Movement Primitives, Learning from Demonstration, Online Path Planning, Tool Deflection Compensation

ÖZ

DİNAMİK HAREKET PRİMİTİFLERİ METODU İLE KATI OLMAYAN ROBOTİK ÇAPAK ALMA MAKİNALARI İÇİN ÇEVRİMİÇİ YÖRÜNGE PLANLAMA

Uğurlu, Musab Çağrı
Yüksek Lisans, Makina Mühendisliği Bölümü
Tez Yöneticisi : Doç. Dr. Erhan İlhan Konukseven
Ortak Tez Yöneticisi : Dr. Öğr. Üyesi A. Buğra Koku

Ekim 2018 , 63 sayfa

Robotik çapak alma, belirli yüzey profillerinin hassas ve tekrarlanabilir işlenmesinde kullanılmaktadır. Ancak, geleneksel çapak alma metotlarından farklı olarak bu robotlar, kullanılan aşıntırıcı takım ve robot kolun kendisinin düşük rijitliğinden dolayı zor bir görev olan çapak kalınlığı bilinmeyen parça üzerinde yörünge planlamasına ihtiyaç duymaktadır. Bu çalışma, çevrimdışı hareket primitivlerinden elde edilen takım eğilme bilgisine göre çapak alma robotunun anlık yörünge planlaması için bir metot sunmaktadır. Önce, çapak alma işlemi sırasında 6 serbestlik dereceli robotun görev ile ilgili hareketleri ve takım ile bilinen iş parçası arasındaki etkileşim kuvvetleri kaydedilir. Sonra lazer tarayıcı ile işlenen bu parçalar taranarak istenen kesme derinliği ile gerçek kesme derinliği arasındaki fark elde edildi. İşlenemeyen kalınlık büyük oranda takımın düşük rijitliğinden kaynaklanmaktadır. Ölçülen kuvvetler algı, kalan malzeme ise eylem olarak seçilerek Dinamik Hareket Primitivleri metodu modifiye edildikten sonra toplanan data ile eğitilir ve takım eğilmesinin tahmininde kullanılır. Lineer ve açısal sapmalar hesaplanarak, işlem sırasında anlık olarak telafi edilir ve takım yörüngesi buna göre ayarlanır. Son olarak, bu metot sonucunda elde edilen

formun hata analizi sonuçları standart çapak alma işlemi, PID kontrollü çapak alma işlemi ve Active Disturbance Rejection kontrollü robotik çapak alma ile karşılaştırılmıştır.

Anahtar Kelimeler: Çapak Alma İşlemi, Hareket İlkeleri, Gösterme ile Öğrenme, Çevrimiçi Yol Planlaması, Takım Esnemesi Telafisi

to my years spent in METU

ACKNOWLEDGMENTS

First and foremost, I would first like to express my sincere appreciation and gratitude to my supervisors Assoc. Prof. Dr. E. İlhan Konukseven and Asst. Prof. Dr. A. Buğra Koku for their continuous support, criticism and invaluable guidance throughout my thesis study.

For their comments and criticism, I would also like to thank to the examining committee members; Asst. Prof. Dr. Kıvanç Azgın, Asst. Prof. Dr. Ali Emre Turgut, and Asst. Prof. Dr. Andaç Töre Şamiloğlu.

I would like to thank my lab mates, Payam Parvizi, Uğur Mengilli, Abdülhamit Dönder, Ömer Okumuş, Kemal Açıkgöz and Masoud Latifi Navid for their immense supports and fruitful knowledge they shared. They were always available to discuss my academic questions regardless of time and condition. I appreciate the sleepless nights we shared to carry on our project.

I would like to express my profound gratitude to my parents, brothers and sister. Their enlightened vision helped me to choose my goals and pursue them. This study would not be finished without their patience, support and encouragements.

Finally, yet importantly, I am gratefully indebted to my colleagues and friends, Sinan Özgün Demir, Tayfun Efe Ertop, Onurcan Kaya, Atae Jafari Tabrizi, Saadet Baltacı, İsmail Özçil, Sedat Pala, Yashar Badienia for their supports and collaborations throughout my thesis study. I appreciate the members of METU Aikido Society, Furkan Taşdemir, Melisa Nur Kart, Hatice Aydın, Selin Ayvalı, Koray Can Yurtseven, Utku Uyar, Melike Yürekli, Mert İşler for sharing their companion and our refreshing activities.

I also would like to thank the Scientific and Technological Research Council of Turkey for their financial support of this research under Grant TÜBITAK- 114E274.

TABLE OF CONTENTS

LIST OF TABLES

TABLES

LIST OF FIGURES

FIGURES

LIST OF ABBREVIATIONS

DMP	Dynamic Movement Primitives
LWR	Locally Weighted Regression
MEAN	Average value of an array
STD	Standard Deviation
RMS	Root Mean Square
ADRC	Active Disturbance Rejection Control
F_n	Normal force
F_t	Tangential force
D_c	Depth of cut
f_R	Feed-rate
v_s	Spindle speed
ω_i	ith weight of nonlinear function
τ_z	Temporal scaling factor
α_z	Time constant
τ_v	Temporal scaling factor
α_v	Time constant
$f(x)$	Nonlinear term of DMP, function of phase variable
$f_{grind}(F_n, F_t)$	Nonlinear term of DMP, funtion of grinding forces
$\psi_i(x)$	ith basis function of nonlinear term
τ_x	Temporal scaling factor
α_x	Constant value
x	Phase variable
h_i	Width of ith basis function
c_i	Center of ith basis function

CHAPTER 1

INTRODUCTION

1.1 Deburring Process

In manufacturing industries, in order to increase the quality of the machined part, final finishing processes are performed. Deburring is one of the final finishing processes that is used mostly in Aerospace structures, Automobile parts and medical implants which the surface quality of machined parts should be functionalized to get more efficient performance. Deburring is a process that removes unwanted small piece of material (burr) remain attached to the surface and edge of machined part. Although burrs are very small in size, they can cause unexpected complications during assembly and early failure since they increase stress on structures in high pressure and etc. [6], [10], [15].

There are various types of deburring process including Manual, Thermal, Electrical. In industry, the most largely used deburring process is manual operation that is depended on skills of human operator. Although human operator is adaptable to perform deburring process on different workpiece surface shapes, in deburring process with micron-size resolution, operators have a lack of dexterity and repeatability in mass productions. Automation can be a solution of above-mentioned problems of human manual operator, Figure 1.1.

Nowadays, by increasing the demand on repeatability and high precision of machined parts in a mass production, robotic deburring process takes the place of the manual deburring. Since deburring robots are not adaptable to various workpiece shapes, it is better to have more study on manual deburring process. Since the generation of action for each given task cannot be programmed for every environmental situation, a

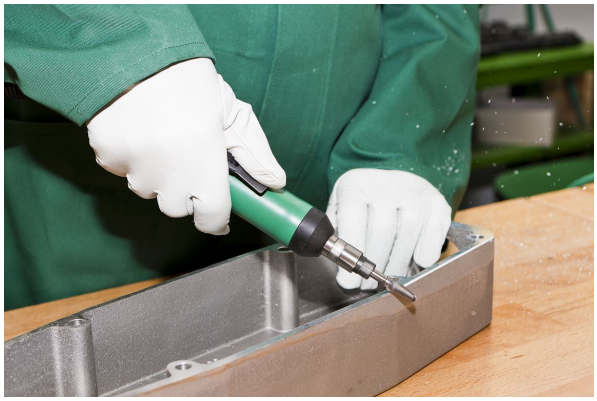

Figure 1.1: Example of manual deburring process

proper general mathematical method can be utilized by using the library of previous experiments performed before.

1.2 Force Interaction

Before generation of mathematical method for every task, the environment and the interaction of robot with environment is required to be known. During deburring process, when spindle tool gets in contact with the workpiece, the interaction force/-moment occurs. By the help of interaction forces, user can have an idea about the workpiece material, depth of cut, feed-rate of robot, tool position and orientation with respect to workpiece and etc. However, in robotic deburring, significant tool deflection occurs due to the lower combined stiffness of the robot, tool and workpiece. Tool deflection during robotic deburring operation changes the position of the tool which is illustrated in Figure 1.2. Therefore, tool cannot achieving the set depth of cut in the workpiece cross section. Also, the orientation of the tool become distorted [14].

In micron-size resolution deburring process, tool deflection has to be compensated in order to eliminate form error and geometrical errors. By utilizing the force/torque sensor, the tool deflection and related created force can be collected. There are many different tool deflection compensation methods. Firstly, This tool deflection can be compensated by assuming the tool as a beam and then applying beam deflection methods. Since the angle and length of the tool are known, kinematic movements on robot

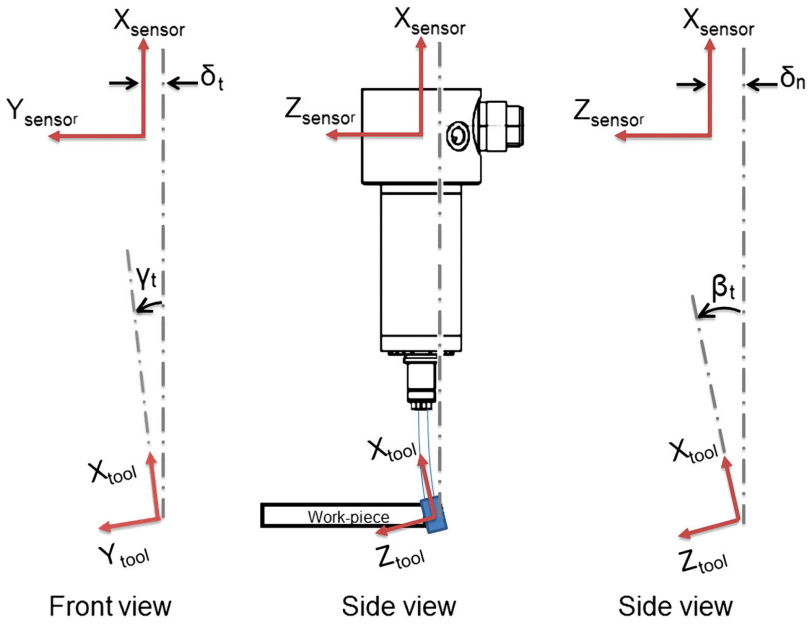

Figure 1.2: Example of tool deflection in light abrasive grinding. Tool deflection errors are δ_n, δ_t, γ_t and β_t [14]

.

can be performed. In addition, this can be embedded into the general mathematical method of task generation.

1.3 Thesis Motivation and Objective

By explaining the concept of manual and robotic deburring processes and the interaction force, one can realize that the main concept of this study is to perform deburring process in micron-size resolution by utilizing non-stiff deburring robot by considering the interaction force between the tool and workpiece.

There is a problem that should be solved in order to provide non-stiff robot to perform deburring process. Deburring forces causes deflections both on the tool and the robotic system, therefore set depth of cut cannot be achieved during the process. In order to solve this problem, a new trajectory should be generated so the required surface profile will be achieved. Therefore, a trajectory generation method would be a solution to this problem.

General motivation of this study is to develop a mathematical method of trajectory by utilizing Dynamic Movement Primitives (DMP). DMP is a method of trajectory generation motivated by the desire to find a way to represent complex motor actions. Also, its structure is very available to include sensory data as a function. It would be a useful tool for adapting the deburring process to a robotic system.

The experimental setup that is used in this study has a force/torque sensor available which can record instantaneously during the deburring process. By utilizing force/-torque data with DMP, online trajectory manipulation can be performed. When force is out of the range of desired range, DMP steps in and gives the new trajectory to robot.

1.4 Thesis Outline

In this thesis, a method for eliminating form errors of workpieces machined by robotic deburring machines is developed and applied. This work is presented as follows:

In chapter 2, literature survey is presented. This chapter includes similar previous studies and also some inspirational studies that are not directly related.

In chapter 3, changes and additions on the classical DMP method to apply DMP to deburring process for online trajectory adjustments are presented and explained.

In chapter 4, experimental setups which are developed and used, and specifications of their components are introduced.

In chapter 5, The DMP method to learn motor skills of human expert performing manual deburring operation is presented. The task-related movements of the human expert are recorded. Then, the intrinsic movement primitives using an ordinary differential equation are parameterized.

In chapter 6, experimental procedure for application of DMP is explained. This application requires a series of experiments to train functions and validate that it is a solution for the form errors.

In chapter 7, the results of the conducted experiments are shared and interpreted.

Also, the results of robotic grinding process with DMP is compared with grinding processes with different controllers.

Finally, in chapter 8, the thesis is concluded by briefly summarizing the work done and discussing possible future work for further development of the methods.

CHAPTER 2

LITERATURE SURVEY

In today's manufacturing, manual grinding process is still the most extensively used grinding process in the industry. This is because human experts who perform the tasks are adaptive to any new tasks and the tools are low-cost. However, by increasing the need for more precise machined parts, the need for adaptive robotic grinding process is increased and replaced with manual grinding process.

This brings the question that how a grinding robot can become adaptive? The robot that will be customized has to be able to understand what to imitate and be capable of mapping the perception coming from ongoing process to desired action in real-time (online). Also, the robot should be able to acquire itself to the new task autonomously and by collecting data sets from ongoing experiments, it must enhance itself to more complex tasks without any additional effort from operator.

Robots can have imitative behavior in order to mimic the demonstrator [22]. This demonstrator can be a human expert or the robot itself. The ability of imitation can be learned based on theoretical deduction or empirical observation. For example, in learning by imitation [7],[24],[4], the robot is supplied to the facility that supports further learning and understanding by imitating the behavior given. When robot learns to imitate, named learning to imitate [2], by performing through repetitive experiments, it can solve the 'Correspondence Problem'. In addition, in learning by demonstration [26],[20], robot performs a new task which may or may not be an imitative behavior. In the case of not having imitative behavior, named task-level imitation, robot learns to perform a task of the demonstration of previous experiments by replicating it, such as robots in mass production and assembly [13]. However, when giving the knowledge of the goal of the task, robots have learned to perform a task [18], [17]

by making use of both the demonstrator's movement and reform movements in order to reach the goal and decrease error to minimum [3]. Figure 2.1 is from paper [17] which was about teaching robot arm to hit the ball by using one of the methods of Learning by Demonstration.

As it is mentioned before, imitative behavior can be transferred from previous experiments of the robot to itself in order to learn and adapt to new task goals. Our problem is to give grinding robot the ability to perform grinding process on workpieces with random surface and unknown chip thickness in micron size resolution. In grinding process, grinding forces causes deflections both on the grinding bits and the robotic system, therefore set depth of cut cannot be achieved during the process. In order to solve this problem, a general method should be generated so the required surface profile can be achieved from any randomly shaped surface profiles. This method should be able to recognize the forces created by burrs and compensate them in order to get desired surface profile of the workpiece. Thus, robot has to use a general method to know how to imitate and to understand what perceptual aspects are related to the task. This imitation of grinding robot can be from human expert demonstrations or from previous experiments of the same robot.

Broadly speaking, there are many general solutions to the problem of perceiving movements, such as Hidden Markov models, motor primitives, division of movements and etc. One of the methods encountered in the literature used for the purpose of skill transfer is presented by S.Liu and H.Asada [16]. In this paper, the hand movements of human operator are modeled by Artificial Neural Network. In this method, the goal is to model each task that is being performed by the expert user during the operation. When a user performs grinding on a certain workpiece, there are two separate tasks: Tool manipulation by the user, and grinding process. The aim is to find a relation between these two tasks. Parameters for simplified models of both tasks are identified and using a nonlinear mapping technique, a mapping between parameters of the two models is created. By inspiring from [16], force interactions and tool movements are the base for representing the robotic grinding process. Hogan's paper [8] claims that each movement can be categorized to three main movement and sub-movements, which are Sub-Movements, Oscillations and Mechanical Impedance. Sub-movements are very simple trajectories defined by a simple math-

ematical function. Their combinations can provide any discrete movement. Oscillations are special combinations of sub-movements and they are used to represent rhythmic movements in the motion. Finally, mechanical impedance is to represent the relation between the forces due to physical interaction and the motion. It is defined as a dynamic operator which gives the force for a given displacement, velocity, acceleration. Furthermore, [12] considers reaction forces as a crucial role on final quality. It underlines learning skills which are focusing on interaction forces rather than kinematics. Based on Kober's study, there are three concepts for learning force interaction skills. First, by using contact information, determination of segments from kinesthetic demonstrations. Second, each segment can be associated with movement primitive. Lastly, by using these movement primitives, transitions between them can be determined.

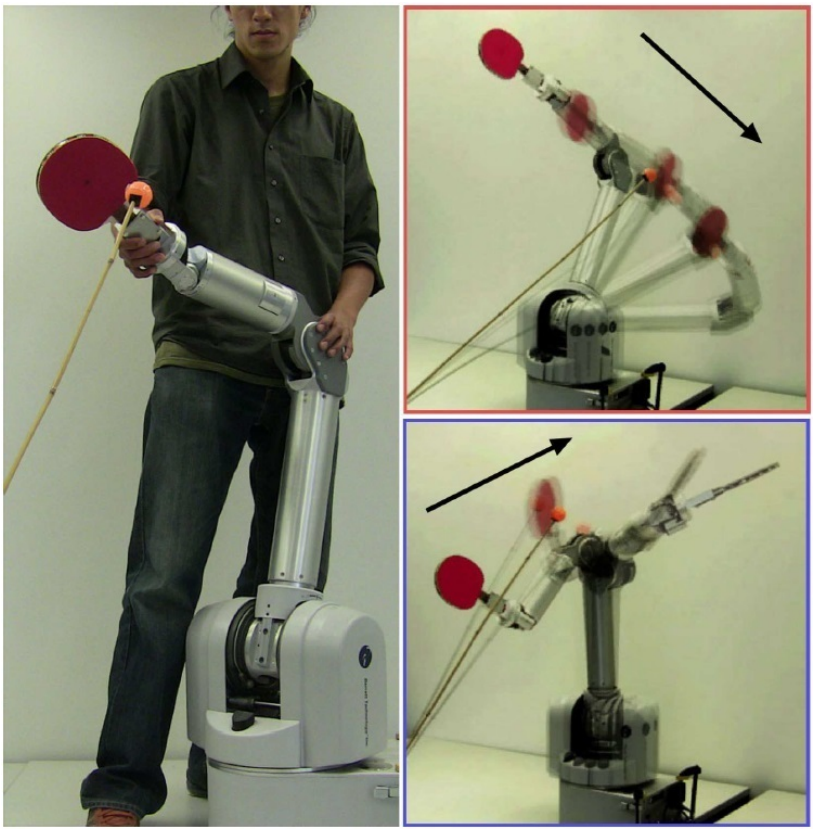

Figure 2.1: Teaching robot arm to hit a ball, "Learning by Demonstration"

Considering papers mentioned, it can be said that splitting movement in Sub-Movements with their velocity and accelerations are actually the Movement Primitives of the movement. Dynamic Movement Primitives (DMP) is one of the methods of general-

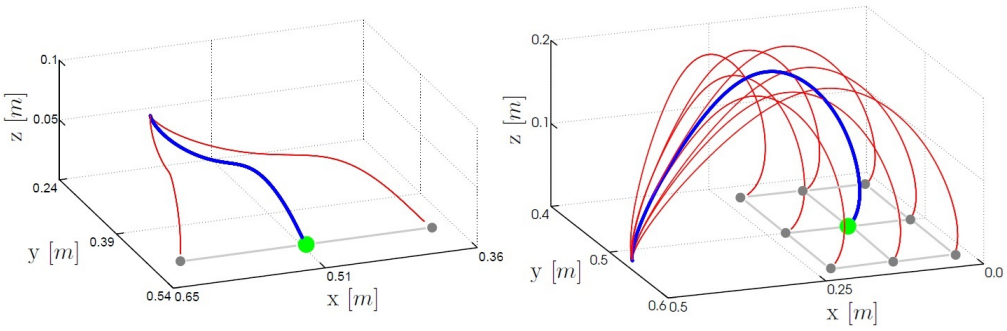

Figure 2.2: Blue lines: The desired trajectory, Red line: Trajectory obtained for different goal positions by DMP.

izing movement primitives which first developed by S.Schaal [23]. Then, in paper of Pastor [20], human grasping and placing movements imitated by robot by using DMP method. In [20], the problem of imitation of human grasping and placing movements by a robot was solved with the help of three challenges: The correspondence problem, generalization, and robustness against perturbation. The links and joints of robot may not match with human arm which is the correspondence problem. In addition, generalization is required to demonstrate every single movement in different situations. In other words, robot should be able to demonstrate the same motion primitive with different start and desired end positions. Finally, robustness against perturbation is another important problem. Environment is not always as perfect as it is thought in which obstacles may appear suddenly in dynamic environment and cause collision of the robot arm. To clarify these problems, DMP model was presented which is able to represent any obstacle avoidance movement with a set of differential equations.

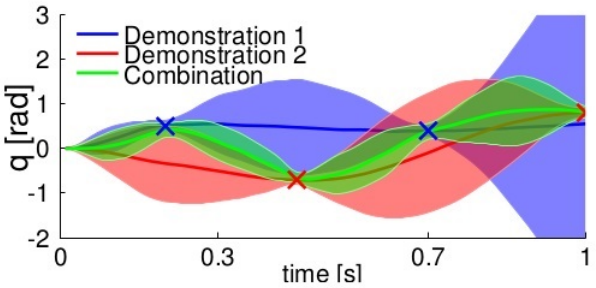

Figure 2.3: Example of Combination of Demonstrations

In Figure 2.2, human hand movements are obtained from experiments from [20] are shown with blue trajectory and the trajectories generated by DMP in different goal positions are in red.

DMP method is not only limited to robot arm and industrial robot movements. For instance, in [21], a framework for learning aggressive obstacle avoidance maneuvers in flight control of UAVs was introduced. Firstly, aggressive maneuvers were imitated by using the data taken from human performed obstacle avoidance maneuver. Having inspired from the data taken during imitation, Dynamic motion primitives (DMP) of the maneuver was introduced and extended using nonlinear contraction theory. In this trajectory model, the complex primitive trajectories were generated by computing the trajectory dynamics in DMP for different start and the desired end positions. Therefore, DMP algorithm can be useful for complex trajectory movements with different start and end positions without considering the model of UAV.

The works about DMP show that the complex trajectory movements with different start and goal positions in high dimensions can be generated. Also, it can be assumed the dynamic environments as interaction forces created during grinding process. Trajectory generation can consider these forces as obstacles to avoid. There are some works that are directly related to our problem. In [1], online trajectory generation by using DMP method on grinding robot is investigated by utilizing teleoperation. Since there is a teleoperation between 1-D setup and grinding robot, the correspondence problem solved automatically. Force trajectories of human expert while doing grinding process in 1-Dimensional setup are extracted to sub-force trajectories (movement primitives). utilizing dataset of movement primitives, DMP can serve as a building block for a human active controller. This building block can prevent forces out of the desired range and move it back to the range.

Moreover, in [19], the specified DMPs (sDMP) approach is introduced. Since the tool of spindle and the workpiece have contact with each other, the nonlinear term of DMP should include contact force term which is related to specific grinding task. This coupling term is multiplied with the resultant force exerted on the tool tip. As reviewed on literature Survey, DMPs are more common in humanoid robots, robot locomotion and robot arm tasks. Although these robots have to perform a task in

dynamic environments, the robots do not need to be highly precise. However, in robotic grinding, the environment can be considered static but the movements have to be precise. The experiments in this work are performed by human participants hand movements on haptic interface. The aim of this paper was to show the ability to apply DMP on high precise grinding robots.

DMP method can be improved by combining with other methods. In [17] a method of Beta Process Auto Regressive Hidden Markov Model (BP-AR-HMM) is combined with DMP model for segmenting demonstrations and generalizing tasks from that unstructured demonstrations. By combining these two methods, a multi-step task can be learned and generalized and it can be given to the potential library to collect skills over time. Moreover, different DMPs taken from different demonstrations can be combined [18], as shown in Figure 2.3.

In our robotic grinding process, surfaces in micron-size resolution have to be obtained. By utilizing from inspiring academic works explained, our motivation is to introduce a new trajectory model by utilizing DMP method. This new method is a tool for generation of trajectory for an unknown chip thickness. The generation of this trajectory is a hard task due to the low stiffness of robot arms and spindle tool and unknown chip thickness.

CHAPTER 3

METHODOLOGY

3.1 Dynamic Movement Primitives

Method of Dynamic Movement Primitives [25] is one of the most promising methods in robotics for the purpose of transferring any kinds of movements to machines. In simple words, using this method, a robot can follow very complex trajectories that is demonstrated to the robot. This method enables the generalization of goal-oriented tasks, such as grasping an object and moving it to a predefined position, while being able to avoid obstacles with any shapes. From dynamical systems point of view, this type of behavior is an attractor behavior, where two points in space are connected to each other via a trajectory. Note that both point attractors and limit cycle attractors are present. Modeling such a behavior is possible by introducing a simple linear differential equation, as a representative of a simple dynamical system, and then transforming it into a weakly nonlinear system by an autonomous forcing term. This way both attractor dynamics and trajectory of the system can be modified. Developed model should be an autonomous one, that is, there should be no explicit dependency on time. This feature enables adding other coupling terms to the main dynamical system (e.g., to avoid obstacles, or to include force control considerations, or to implement closed-loop perception-action systems).

The most basic linear dynamical system, which can be used as a model is a mass-spring-damper system. This model is actually very suitable for motor control problems, which are most commonly described by second-order differential equations and require position, velocity and acceleration information for control. The model is writ-

ten as,

$$\tau_z \ddot{y} = \alpha_z(\beta_z(g - y) - \dot{y}) + f(x) \tag{3.1}$$

Where τ is a time constant, and α_z and β_z are positive constants. And $f(x)$ is the forcing term. In this context, the variables y, $\dot{y}$, $\ddot{y}$ are interpreted as desired position, velocity and acceleration for a control system, and a controller will convert these variables into motor commands.

To make things easier, model will be rewritten in first-order notation as,

$$\tau \dot{z} = \alpha_z(\beta_z(g - y) - z) + f(x) \tag{3.2}$$

$$\tau \dot{y} = z \tag{3.3}$$

This system is called "transformation system", since it transforms simple dynamics of unforced systems into a desired nonlinear behavior. Note that if the forcing term is fixed to zero then the equation represents a globally stable second-order linear system where

$$(z, y) = (0, g) \tag{3.4}$$

The point above is a unique point attractor. A phasic forcing term will result in a point attractive system, where the trajectory will end at the specified final point. On the other hand, a periodic forcing term will result in an oscillator, that is, in a limit cycle behavior.

Note that since the nature of the system is based on a mass-spring-damper system, the trajectory between the two points might have an underdamped behavior, which obviously is not an efficient trajectory to follow, when the goal is to minimize the time. Therefore, if the positive constants α_z and β_z are tuned such that the system is critically damped, then the trajectory will monotonically converge toward goal (i.e. g). The system can be made critically damped if $\beta_z = \frac{\alpha_z}{4}$.

To be able to modify this simple trajectory, as mentioned above, a nonlinear function, called forcing term is required. This function must be designed such that it is possible to modify it later by a learning algorithm. Therefore, it is obvious that some kind of an arbitrary nonlinear function with adjustable "weights" is suitable for this application. It is a well-established methodology in machine learning to represent arbitrary nonlinear functions in form of linear combination of basis functions. The same procedure can be applied in this case too. Forcing function can be chosen as,

$$f(t) = \frac{\sum_{i=1}^{N} \psi_i(t)\omega_i}{\sum_{i=1}^{N} \psi_i(t)} \tag{3.5}$$

Where ψ_i are fixed basis functions and ω_i are adjustable weights. The parameters ω_i can be adjusted using learning algorithms in order to produce complex trajectories before reaching g. Forcing term introduced in this form has a problem, and it is its explicit time dependency. The explicit time dependence of this non-linearity creates a non-autonomous dynamical system. And as mentioned previously, such a system does not allow straightforward coupling with other dynamical systems. Therefore a replacement of time by means of a first-order linear dynamics is introduced as,

$$\tau \dot{x} = -\alpha_x x \tag{3.6}$$

Where α_x is constant. Starting from some arbitrarily chosen initial state x_0, such as $x_0 = 1$, the state x converges monotonically to zero. Thus x can be conceived of as a phase variable, where $x = 1$ would indicate the start of the time evolution and x close to zero means that the goal g has essentially been achieved. For this reason, it is important that $x = 0$ is a stable fixed point of these equations. This equation is called "canonical system" because it models the generic behavior of the model equations.

Therefore forcing function can be reformulated as,

$$f(t) = \frac{\sum_{i=1}^{N} \psi_i(t)\omega_i}{\sum_{i=1}^{N} \psi_i(t)} x(g - y_0) \tag{3.7}$$

With N exponential basis functions $\psi_i(x)$ is

$$\psi_i(x) = \exp\left(-h_i(x - c_i)^2)\right) \tag{3.8}$$

Where h_i and c_i are constants that determine the width and centers of the basis functions respectively, and y_0 is the initial state $y_0 = y(t = 0)$.

Note that the forcing term introduced above is modulated by both x and $(g - y_0)$. The modulation by x means that the forcing term effectively vanishes when the goal g has been reached; an essential component is proving the stability of the attractor equations. The modulation by $(g - y_0)$ will lead to useful scaling properties of our model under a change of the movement amplitude $(g - y_0)$.

The complete system is designed to have a unique equilibrium point at $(z, y, x) = (0, g, 0)$. Recall that $\tau\dot{y} = z$, and $x = 0$ means that g is reached.

Thus, it has been shown that with modifying the weights of the forcing term, it is possible to generate complex trajectories until it reaches the point attractor g. These complex trajectories will be generated in order to make the robot follow the complex and nonlinear trajectories.

If it is required to model the limit cycle behavior, instead of a point attractor, a similar approach is followed. Obviously, a periodicity must be introduced into the system. This periodicity can be introduced either in canonical system or the basis function. Latter method is more convenient; therefore it will be shown here.

A phase oscillator for learning limit cycle can be used.

$$\tau\dot{\phi} = 1 \tag{3.9}$$

Where $\phi \in [0, 2\pi]$ is the phase angle of the oscillator (in polar coordinates) and the amplitude of the oscillation is assumed to be r. Forcing term can be created as,

$$f(\phi, r) = \frac{\sum_{i=1}^{N} \psi_i \omega_i}{\sum_{i=1}^{N} \psi_i} \tag{3.10}$$

Where,

$$\psi_i = \exp\left(h_i\left(\cos(\phi - c_i) - 1\right)\right) \tag{3.11}$$

Exponential basis functions, in this case, are von Mises basis functions, which are actually Gaussian-like functions that are periodic.

If such a forcing term is used in the transformation system, then the goal point g will be a point where the trajectory will eventually follow the limit cycle around it. It can be interpreted as an anchor point for the oscillatory trajectory, which can be changed to accommodate any desired baseline of the oscillation. The amplitude and period of the oscillations can be modulated in real time by varying r and τ respectively.

3.1.1 Training Procedure

Learning procedure of the system will be finalized by adjusting the weights of the forcing term. During the learning procedure, there are two separate phases to be performed. First, the high-level parameters will be determined. High-level parameters are g, y_0, and τ for the discrete movement, and g, r, and τ for the rhythmic movement.

Note that for the discrete movement the parameter g is the final position of the movement, and y_0 is the initial position. And the time constant τ must be adjusted to the duration of the demonstration. For the rhythmic movement g is an anchor point, that is, it is the mid-position of the rhythmic movement. The parameter is chosen to be the period of the rhythmic movement that is demonstrated divided by 2π. The parameter r is used to modulate the amplitude of the oscillations, can be chosen to be 1.0, without loss of generality.

In the next phase, the learning phase for estimating the weights will be performed. Any function approximator can be used for this purpose. A useful learning method specific for the purpose of this work is locally weighted regression (LWR). It is a very fast learning method, and it helps to result in a stable parameterization that can

be used for movement recognition. Rearrange the transformation system 3.2 as

$$\tau\dot{z} - \alpha_z \left(\beta_z(g - y) - z\right) = f \tag{3.12}$$

During the demonstration session following information are to be recorded.

$$\left(y_{demo}(t), \dot{y}_{demo}(t), \ddot{y}_{demo}(t)\right), \text{ where } t \in [1, \ldots, P] \tag{3.13}$$

Where $g = y_{demo}(P)$ and $y_0 = y_{demo}(0)$. After determining the high-level parameters, the following relation can be obtained.

$$f_{target} = \tau^2\ddot{y}_{demo} - \alpha_z \left(\beta_z(g - y_{demo}) - \tau\dot{y}_{demo}\right) \tag{3.14}$$

After obtaining the relation above, the goal is to fit the weights in forcing term, so that it is as close as possible to f_{target}. LWR algorithm fits for each basis function in the forcing term a corresponding weight.

3.1.2 Using DMP for Multi-DoF Systems

So far, DMP method is explained for 1-DoF systems. When applying DMP for multi-DoF systems, each DoF requires a separate transformation system whose form is given in (3.2) and (3.3), however, to maintain coordination there should be only one canonical system. By this way, on each DoF motion can be planned with a different forcing function and synchronized movements can be achieved since these functions take the same phase variable from one canonical system (See. Figure 3.1) [9].

3.2 Modifications on DMP

In the content of this thesis, DMP was used to compensate the deflections and angular deviations of the tool tip which obviously cause form error on the workpiece. Therefore, there were two transformation systems with extra nonlinear functions are used to add force/torque data to the system as perceptions.

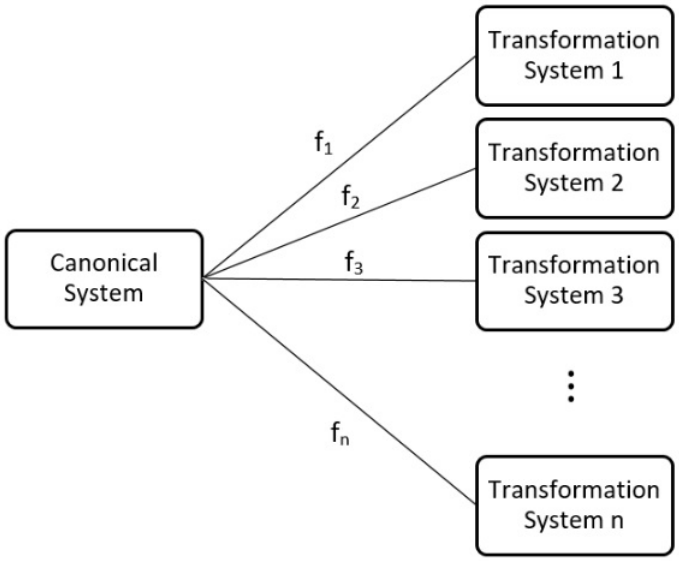

Figure 3.1: Application schematic of DMP on multi-DoF systems

As mentioned in section 3.1.2, in application, each DoF of the system need to be modeled with separate DMPs, that is, transformation systems. Although, the robotic grinding setup is 6-DoF (Figure 4.2), in the operation there are 4-DoF since the translational movement along the tool (x-axis) and rotation about the tool (u-axis) are not effective on the process and excluded. Therefore, there are two translational movements in normal and tangential directions of the cutting operation and two rotational movements about these axes are considered to be manipulated by DMP. Then, general formulation for the translational coordinates of the tool becomes as,

$$\tau \dot{z} = \alpha_z(\beta_z(g - y) - z) + f(x) + f_{grind}(F_n, F_t) \tag{3.15}$$

This extra nonlinear function is containing the information of process behavior. It has the force feedback as perception therefore, the coupling term should be a function of grinding forces. This new function is,

$$f_{grind}(F_n, F_t) = \frac{\sum_{i=1}^{N} \psi_i(F_n, F_t)\omega_i}{\sum_{i=1}^{N} \psi_i(F_n, F_t)} \tag{3.16}$$

Where, ω_i's are weights and $\psi_i(F_n, F_t)$'s are basis functions in a form similar to (3.7). During the process it is assumed that the location of the workpiece is known, but the

burrs or the amount of material to be removed is unknown so the forces can not be predicted before the process. Therefore, the relation between the deflections/deviations and the forces should be learned to make adjustments on the trajectory. In other words the functions below should be extracted,

$$\delta = f(F_n, F_t) \tag{3.17}$$

$$\theta = f(F_n, F_t) \tag{3.18}$$

Where, δ is the deflection and θ is the angular deviation of the tool tip. Finally, the transformation system is turned into the below form.

$$\tau \dot{z} = \alpha_z(g - z) + f(x) + f_{grind}(F_n, F_t) \tag{3.19}$$

Here the order of the transformation system is reduced to one to make the system more responsive and get rid of the effects of second order behavior. In this equation z is the generalized coordinate and can represent any parameter in the system to be manipulated.

CHAPTER 4

EXPERIMENTAL SETUP

4.1 Introduction

As it is mentioned before, the aim of this thesis is to have grinding process with desired depth of cut. In order to determine the accuracy of the depth of cut in on-line grinding processes, several experimental setups and devices are obtained. The main experimental setup utilized in this work is robotic grinding setup. This robot is developed for performing grinding/deburring process in micron-size resolution in controlled environment. The workpiece position in this setup is defined before, however, the shape of the surface of the workpiece may or may not be defined. This setup is also capable of measuring the form change and roughness of the surface of the workpieces.

In addition, in order to record the movements and forces created by human operator while performing grinding process, the motion primitives experimental setup is built. For recording the hand and wrist movement of the operator the haptic device is used. Also, by utilizing the 6-DOF force/torque sensor, the forces exerted while performing the grinding process by operator can be recorded and collected.

Finally, before and after performing grinding process, we can measure the surface of the workpiece on manual measurement setup. By the help of the point laser scanner available in the setup, we can measure the surface roughness and form changes of machined workpieces. As it is mentioned before, surface measurement can also be performed by robotic grinding setup.

4.2 Robotic Grinding Setup

This setup contains of 6-DoF parallel manipulator (Hexapod), a Force/Torque sensor, a spindle, a point laser scanner and workpiece. The 6-DoF parallel manipulator is attached to a fixed metal and has a free space to move in controlled environment. Also, The spindle, which is attached to the front plate of the Hexapod, turns a tool for performing machining process. While the process, the F/T sensor which is attached to spindle can read and record force and torques created. An overall appearance of the robotic grinding setup is shown in Figure 4.1.

Note that, the spindle can be replaced by point laser scanner. In order to attach the spindle and laser scanner to Hexapod, there is a tool changer component that allows mounting and demounting the spindle and laser scanner. Therefore, the setup can have two configurations. One of them is to perform grinding with force feedback, and the other is laser scanning for measuring the surfaces and edges of the workpiece attached on the table. The robotic grinding setup while doing measurement with point laser scanner is shown in Figure 4.2.

4.2.1 6-DoF Parallel Manipulator

PI H-824.G1 Hexapod is the main device in the setup that carries other components of the setup. It is mounted on a chassis composed of sheet metal and extruded aluminum parts. This device moves the tool, that is attached to the spindle, in a desired direction and orientation in a limited environment.

Some of its specifications are,

- Min. incremental motion X, Y, Z: 0.3 µm
- Min. incremental motion A, B, C: 3.5 µrad
- Repeatability X, Y: $\pm$ 0.5 µm
- Repeatability Z: $\pm$ 0.15 µm
- Max. velocity X, Y, Z: 1 mm/s

- Max. Load: 10 kg
- Connection type: Ethernet

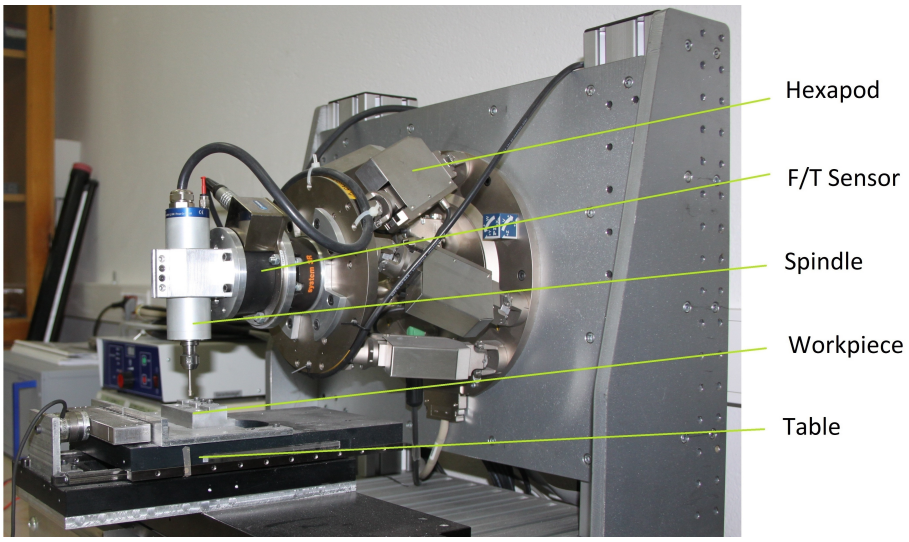

Figure 4.1: Overall appearance of robotic grinding setup

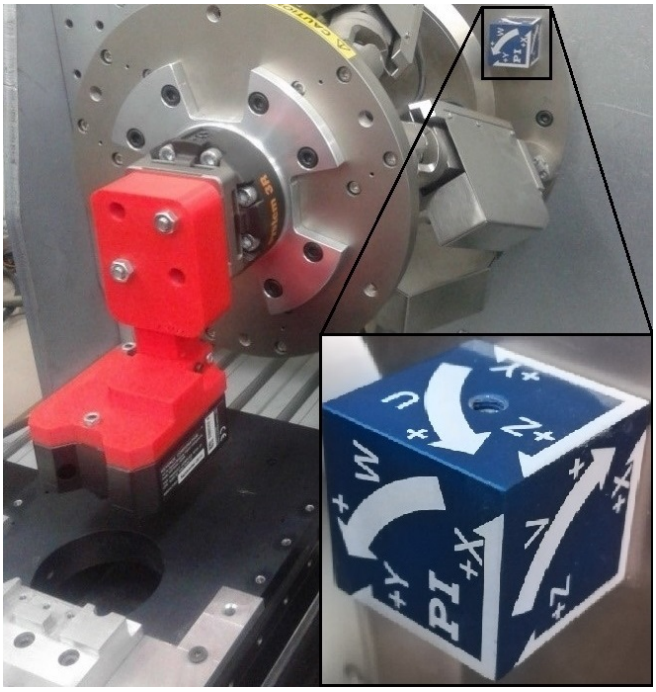

Figure 4.2: Grinding robot with point laser scanner attached and the coordinate frame of the setup.

Figure 4.3: System 3R-628.24-S Macro Starter Package. Part names from left to right: Table chunk, Draw-bar, and Pallet

Figure 4.4: ATI Gamma IP60 force/torque sensor

Figure 4.5: BMR Company's 222-42-MHM Spindle and SFU 0200 Frequency Converter.

4.2.2 System 3R

3R-628.24-S Macro Starter Package is placed on the front surface of the Hexapod robot to mount and demount different end effectors with a repeatability of 0.002 mm without impairing calibration, e.g. spindle and scanner. The package has three parts and they are shown in Figure 4.3.

4.2.3 F/T Sensor

In order to measure forces and torques on the spindle, an ATI Gamma IP60 force/-torque sensor was utilized (See. Figure 4.4). It carries the spindle and records all the forces and torques exerted on the machining tool.

Some of its specifications are,

- Sensing ranges Fx, Fy: $\pm$ 32 N
- Sensing range Fz: $\pm$ 100 N
- Sensing ranges Tx, Ty, Tz: $\pm$ 2.5 Nm
- Resolution X, Y: 0.00625 N
- Resolution Z: 0.0125 N
- Resolution Tx, Ty, Tz: $\pm$ 0.0005 Nm

4.2.4 Spindle

BMR Company's 222-42-MHM Spindle and SFU 0200 Frequency Converter were implemented on the setup to power-up the grinding tools (See. Figure 4.5). The Frequency controller can be adjusted manually or from computer using serial communication.

Some of its specifications are,

- Max. nominal output power: 0.3 kW

- Max. rotation speed: 60,000 rpm
- Weight: 1 kg
- Housing diameter: 42 mm

4.2.5 Point Laser Scanner

Keyence LK-H008 model was utilized on the setup to measure the surface of the workpieces without detaching it from the table, shown in Figure 4.2. When point laser scanner reflects on the workpiece, it creates line because of distance, then, it automatically takes the average distance of the line and gives one distance.

Some of its specifications are,

- Spot diameter (at standard distance): 20 µm
- Repeatability: 0.005µm
- Sampling cycle: 2.55-1000 µs (9 steps)
- Measuring distance: 8 mm
- Measuring range $\pm$0.5 mm
- Controller: Keyence LK-H027
- Connection type: RS232

4.3 Motion Primitives Experimental Setup

The motion primitives experimental setup was built for recording the movements of a deburring operator and the forces of the process simultaneously. Therefore, the setup consists of a 6-DoF haptic device to record the hand movements of the operator in 6 axes, a pneumatic spindle is mounted at the last link of the haptic device, and a force/torque sensor to sense the forces when the operator executing the grinding operation. The 6-DOF force/torque sensor is attached to fixed and heavy fixture.

This fixture is attached to table by rubber glue in order to reduce the disturbance to minimum. The overall configuration of motion primitives setup is shown in Figure 4.6.

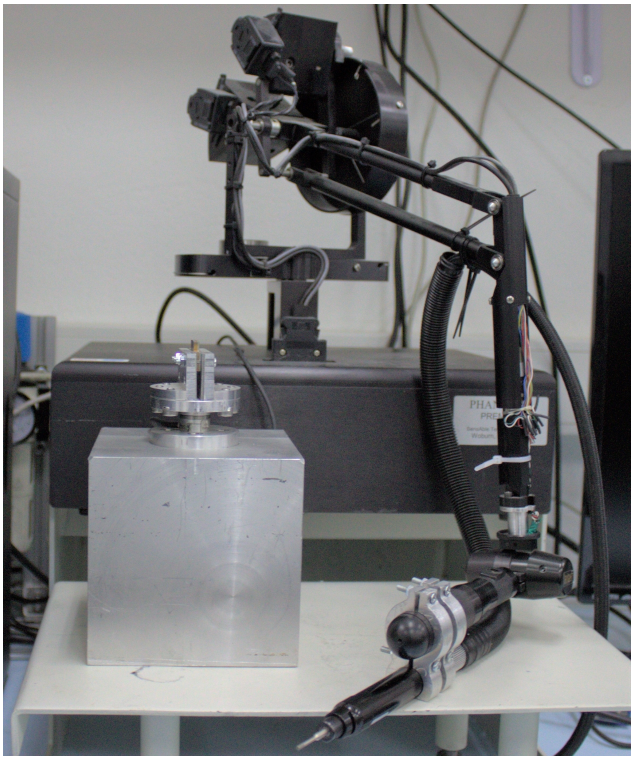

Figure 4.6: Overall appearance of motion primitives experimental setup

4.3.1 6-DoF Haptic Device

A Phantom Premium 6-DoF haptic device was used in this setup to record hand movements of deburring operator. Since there is an encoder stylus gimbal available in this device, we can also record time, directions and orientations of operator during the experiments. Thus, we can also calculate the angular velocities and accelerations of human operator (See. Figure 4.7).

Some of its specifications are,

- Workspace: 381 W x 267 H x 191 D mm
- Nominal position resolution X, Y, Z: 0.03 mm

Figure 4.7: 3D Systems Phantom Premium 1.0

- Nominal position resolution Yaw, Pitch: 0.0023 degrees
- Nominal position resolution Roll: 0.0080 degrees
- Connection interface: Parallel Port

4.3.2 Pneumatic Spindle

Pneumatic Spindle is a device which is connected to compressor from one side and to the machining tool from the other side. The air coming from compressor goes to spindle and rotates the tool. We can control the rotation speed of machining tool by using the apparatus of spindle.

Some of its specifications are,

- Collet size: 3 mm
- Inlet air pressure: 90 PSI
- Unloaded speed: 70,000 rpm
- Housing diameter: 15.4 mm

Figure 4.8: APAC A11-D3105 High Speed Mirco Die Grinder

4.3.3 F/T Sensor

In order to measure forces and torques on the workpiece, an ATI FT07638 force/-torque sensor was utilized. It can be seen from Figure 4.9 that the F/T sensor is fixed below the workpiece. During the deburring/grinding process, when machining tool touches the workpiece, F/T sensor reads and records the moments and forces exerted.

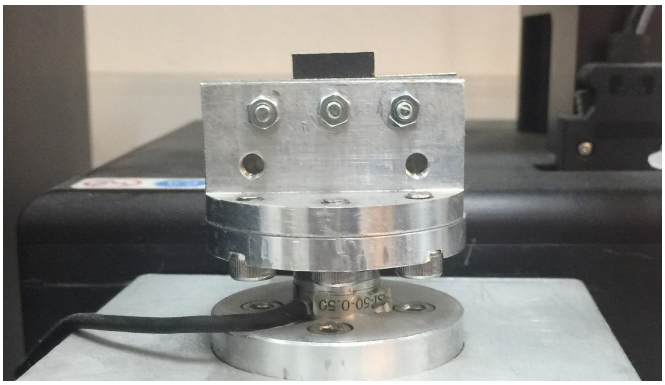

Figure 4.9: ATI FT07638 force/torque sensor(below) with the workpiece fixture(above) calibration SI-50-0.50

4.4 Manual Measurement Setup

The manual measurement setup is built in order to calculate the form change, roughness and amount of the removed material of the surface of the workpiece before and after the experiments. As shown in the Figure 4.10, the manual measurement setup

consists of point laser scanner and 3-DOF positioning device. The laser scanner is fixed and calibrated on the positioning device and reflects on the workpiece. Thanks to precise 3D positioning device, point laser scanner can reach to any position of the surface of the workpiece.

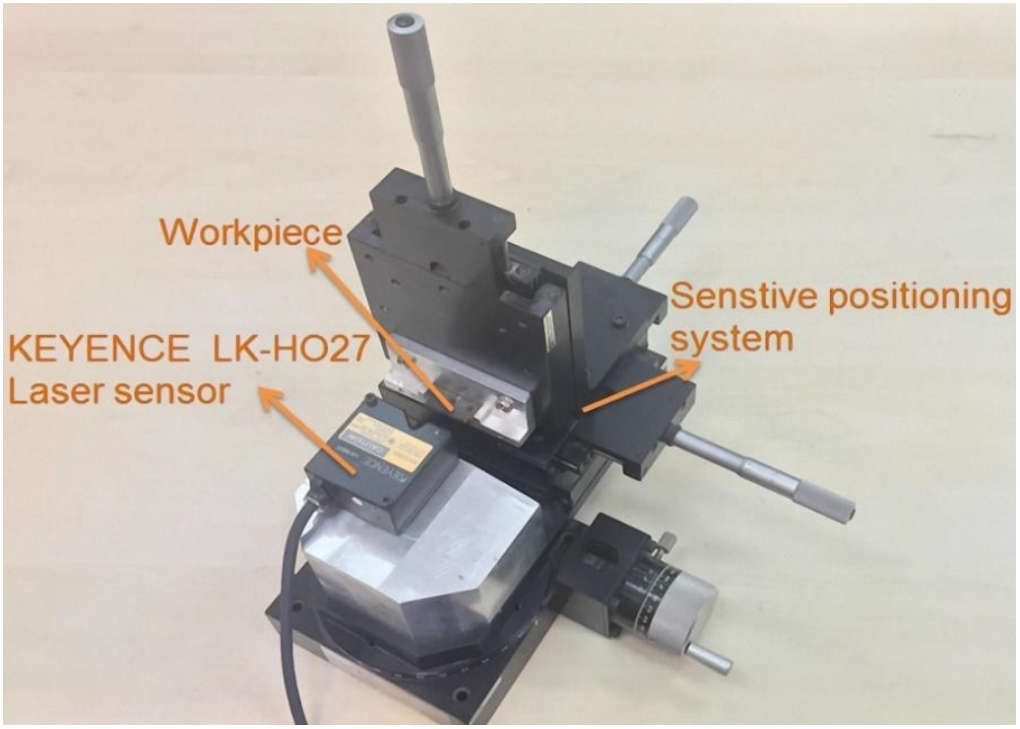

Figure 4.10: Overal appearance of manual measurement setup

4.4.1 Point Laser Scanner

The model of the point laser scanner utilized in this setup is Keyence LK-H027 (Figure 4.10). This scanner can measure from 17 mm to 23 mm and has a 0.02 µm repeatability.

CHAPTER 5

LEARNING HUMAN SKILL MOVEMENT PRIMITIVES

This chapter presents a new method to learn motor skills of human expert performing manual deburring operation. The task-related movements of the human expert are recorded using a haptic device. Then by using an ordinary differential equation of DMP, the intrinsic movement primitives are parameterized. In this study, DMP is used to extract the trajectory of the cutting tool interacting with the workpiece. This trajectory contains the complex behaviors of the human expert. In order to model human expert's movements for precise robotic deburring process, DMP is modified by addition of a non-linear function of deburring forces. Parameters of the modified DMP model are estimated using two-layer feed-forward network, trained by Bayesian regularization back-propagation algorithm. As it is known, these parameters are used to generate human expert like movements for the precise robotic deburring.

5.1 Introduction

In manual deburring, human expert has specific performance during the movement of tool on the workpiece. Experts have exclusive performance in using their wrist and hand motions with the help of their specialized senses, such as understanding surface roughness by touching workpiece surface, listening to the sound of the process for hardness of material, using vision to understand the surface roughness and material removal rate. Similar to manual deburring experts, deburring robots can have possible senses of vibration, vision, sound and Force/Torque (F/T) sensors. Due to physical interaction, F/T sensors are essential as they provide the primary information related to process. Vision can provide valuable information about the overall trajectory but

still this trajectory could not be in micron-size precision and in machining processes generally the trajectory can only be known from the CAD model of the workpiece. Additionally, any visual sensor could not sense machined area during the process. Using force, vibration and sound sensors, characteristics of the process can be distinguished. Within these senses F/T is essential to understand what is happening during the deburring process, other can be an option for further enhancements. Therefore, in this study by using Force/Torque sensors it is planned to transfer the motion primitives of the human expert skills to the robot for trajectory generation to be used in deburring or precise grinding processes. Since the generation of a path for a task cannot be programmed for every situation, DMP which is a general trajectory generation method can replace the traditional methods.

5.2 Methodology

As it is known from the literature survey, chapter 2 and methodology, chapter 3 analyzed before, DMP is more common in locomotion of robots and humanoid robot arm tasks, such as jumping robots, grasping and placing movements. In these tasks, there is a dynamic environment and the movements of robots do not need to have a micron size precision. However, in deburring process used in this study, the environment is static and the trajectory of the tool tip must perform high precision machining on the workpiece. In addition, instead of obstacle avoidance, deburring forces required to be taken into account in deburring process because of the contact between the tool tip and the workpiece which affect the trajectory. Therefore, in this case, coupling term is calculated using deburring forces.

The performed deburring process has two degrees of freedom: depth of cut direction and feed direction. Therefore, to execute this motions, there need to be two different transformation systems.

In [20], the motion primitives were found using weighted summation of the kernel functions, time constants, and time scaling factor were used as the guidance on how to generate the given trajectory. In canonical form, x was used for gating the effect of force term. Here, as an alternative, we propose to augment DMP equation and try to

fit the characteristics of the trajectory to time constants and time scale factors under the influence of current deburring forces.

Therefore, transformation system of the normal motion can be modified to

$$\tau_D \dot{z} = \alpha_D(\beta_D({D_c}^{set} - D_c) - z) + {f_D}^{DMP}(x) + {f_D}^{Deburring}(F_n, F_t) \tag{5.1}$$

$$\tau_D \dot{D}_c = z \tag{5.2}$$

Here, D_c is the depth of cut in the deburring process. Also, the transformation system of the tangential motion on the trajectory is as below:

$$\tau_f \dot{f}_R = \alpha_f(\beta_f(g - p) - z) + {f_f}^{DMP}(x) + {f_f}^{Deburring}(F_n, F_t) \tag{5.3}$$

$$\tau_f \dot{p} = f_R \tag{5.4}$$

Where g is the scaled goal position of the trajectory and p is directly proportional to the position of the tool with Scaling factor, τ_f and f_R is the feed rate of the process.

In both DMPs there are two types of nonlinear functions, which ${f_D}^{DMP}(x)$ and ${f_f}^{DMP}(x)$ are nonlinear forcing term for fitting the trajectory and ${f_D}^{Deburring}(F_n, F_t)$ and ${f_f}^{Deburring}(F_n, F_t)$ are nonlinear functions determined using two-layer feed-forward network that are trained by Bayesian regularization back-propagation algorithm where F_n and F_t are the deburring forces in normal and tangential directions, respectively. Since both of the transformation systems uses F_n and F_t, they have an implicit coupling between each other.

For formulating a function approximation problem, we rearrange (5.1) and (5.3) as

$$\tau_D \dot{z} - \alpha_D(\beta_D({D_c}^{set} - D_c) - z) = {f_D}^{DMP}(x) \tag{5.5}$$

$$\tau_f \dot{f}_R - \alpha_f(\beta_f(g - p) - f_R) = {f_f}^{DMP}(x) \tag{5.6}$$

Inserting the information from the demonstrated trajectory in the left-hand side of the above equations, we obtain;

$$f_{D,target}^{DMP}(x) = {\tau_D}^2 \ddot{D}_c - \alpha_D(\beta_D({D_c}^{set} - D_c) - \tau_D \dot{D}_c) \tag{5.7}$$

$$f_{f,target}^{DMP}(x) = {\tau_f}^2 \dot{f}_R - \alpha_f(\beta_f(g - p) - f_R) \tag{5.8}$$

Thus we have obtained a function approximation problem where the parameters of $f_D^{DMP}(x)$ and $f_f^{DMP}(x)$ are to be adjusted such that $f_D^{DMP}(x)$ and $f_f^{DMP}(x)$ are as close as possible to $f_{D,target}^{DMP}(x)$ and $f_{f,target}^{DMP}(x)$.

The cost function that is used to minimize the error is:

$$J_{Di} = \sum_{t=1}^{P} \psi_i(t)(f_{target}^{D}(t) - \omega_{Di}\xi_D(t))^2 \tag{5.9}$$

$$J_{f_i} = \sum_{t=1}^{P} \psi_i(t)(f_{target}^{f}(t) - \omega_{f_i}\xi_f(t))^2 \tag{5.10}$$

where the exponential basis function is,

$$\psi_i(x) = exp(h_i(x - c_i)^2) \tag{5.11}$$

ω_{Di} and ω_{f_i} are the solution of the linear regression problem which have the equation of below;

$$\omega_i = \frac{\mathbf{s}^T \mathbf{\Gamma}_i \mathbf{f}_{target}}{\mathbf{s}^T \mathbf{\Gamma}_i \mathbf{s}} \tag{5.12}$$

where

$$s = \begin{bmatrix} \xi(1) \\ \xi(2) \\ \vdots \\ \xi(P) \end{bmatrix} \tag{5.13}$$

where $\xi_D(t) = x(t)(g - p)$ and $\xi_f(t) = x(t)(D_c^{set} - D_c)$ and,

$$\Gamma_i = \begin{bmatrix} \psi_i(1) & & & 0 \\ & \psi_i(2) & & \\ & & \ddots & \\ 0 & & & \psi_i(P) \end{bmatrix} \tag{5.14}$$

By using above equations in this part, the forcing terms are obtained, therefore, the generated path is fitted to the trajectory.

The Nonlinear terms of DMP method in tangential and normal directions become

$$f_D^{DMP}(x) = \frac{\sum_{i=1}^{k} \psi_i(x)\omega_i}{\sum_{i=1}^{k} \psi_i(x)} x(D_c^{set} - D_c(0)) \tag{5.15}$$

$$f_f^{DMP}(x) = \frac{\sum_{i=1}^{k} \psi_i(x)\omega_i}{\sum_{i=1}^{k} \psi_i(x)} x(g - p_0) \tag{5.16}$$

Nonlinear equations of $f_D^{Deburring}(F_n, F_t)$ and $f_f^{Deburring}(F_n, F_t)$ can be obtained using the information of demonstration, F_t and F_n to improve the fitting made using only the nonlinear equations of $f_D^{DMP}(x)$ and $f_f^{DMP}(x)$.

$$f_{D,target}^{Deburring}(F_n, F_t) = \tau_D^2 \dot{D}_c - \alpha_D(\beta_D(D_c^{set} - D_c) - \tau_D \dot{D}_c) - f_D^{DMP}(x) \tag{5.17}$$

$$f_{f,target}^{Deburring}(F_n, F_t) = \tau_f^2 \dot{f}_R - \alpha_f(\beta_f(g - p) - f_R) - f_f^{DMP}(x) \tag{5.18}$$

These non-linear functions are approximated using two-layer feed-forward neural network that are trained by Bayesian regularization back-propagation algorithm by using MATLAB Neural Network Toolbox [11]. Considering the offered methods in [27], the number of hidden neurons of neural network is determined.

5.3 Results

In this section, the trajectory of the tool tip of the haptic device on the flat profile of the workpiece is examined and the hand motions of human expert are imitated. The task of the participant is to obtain a horizontal flat surface (Figure 4.9). In the experiment, tool tip positions and F/T data is recorded. Then, by using DMP model, a curve fitting of experimental data is obtained. After that, by utilizing the parameters of DMP model, the movements for different attractor points were imitated. For simplicity, we considered tool tip movement only in the tangential and normal direction and used F/T sensor data in tangential and normal direction. It is verified that the trajectory in the experiment and the trajectory obtained from DMP model are compatible.

Figure 5.1 shows the errors of estimated paths with DMP from the actual Path in normal direction while Figure 5.2 shows the errors of estimated paths with DMP from the actual Path in tangential direction with respect to time. In each figure, red lines show error of estimated path using DMP and blue lines error of estimated path using DMP with grinding forces. Figure 5.3 shows the trajectories on the 2D workspace. Where, red solid line is the curves belonging to the actual path followed by the participant, blue solid line is the curves obtained using (5.5) and (5.6), and dashed line is the trajectory generated from (5.1) and (5.3).

In normal direction (5.1) and (5.5) gives very similar results but mean square error from the actual path of DMP with deburring forces is a little smaller than that of original DMP. The mean square error values are 0.0512 and 0.0532 for the two models. However, in tangential direction (5.3) gives better fit with respect to (5.6). The mean square error from the actual path is 33% lower for the DMP with deburring forces with the error values, 0.2783 and 0.4154.

Figure 5.3 shows the trajectories in both tangential and normal directions. As it can

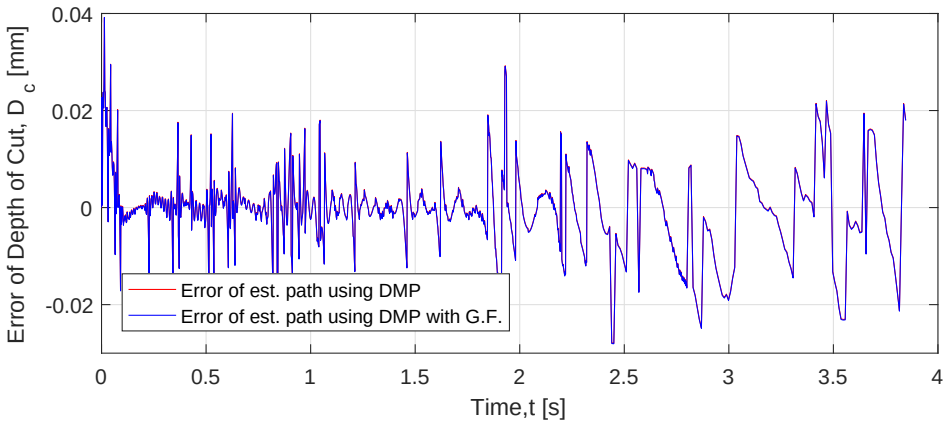

Figure 5.1: Errors of estimated paths with DMP from the actual Path in normal direction.

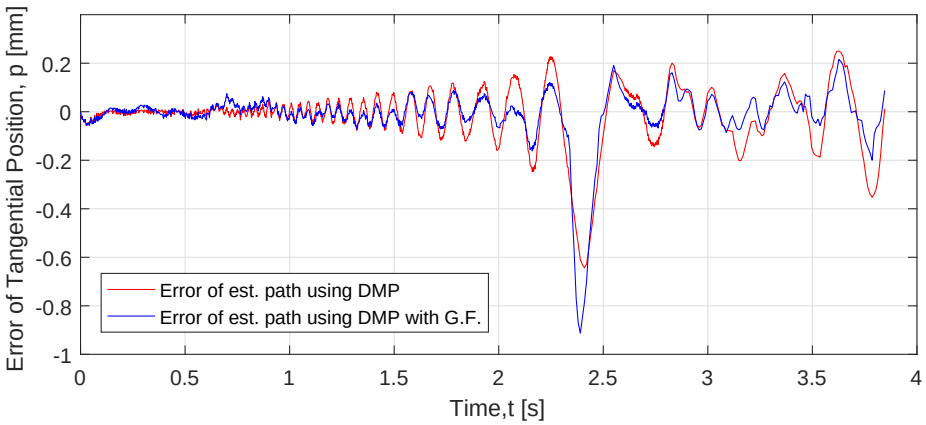

Figure 5.2: Error of estimated paths with DMP from the actual Path in tangential direction.

be seen, estimations using the original DMP and DMP with deburring forces both fit actual path very well. Although, the difference cannot be seen clearly from the figure, the mean square errors are small enough for the imitation of the desired movements.

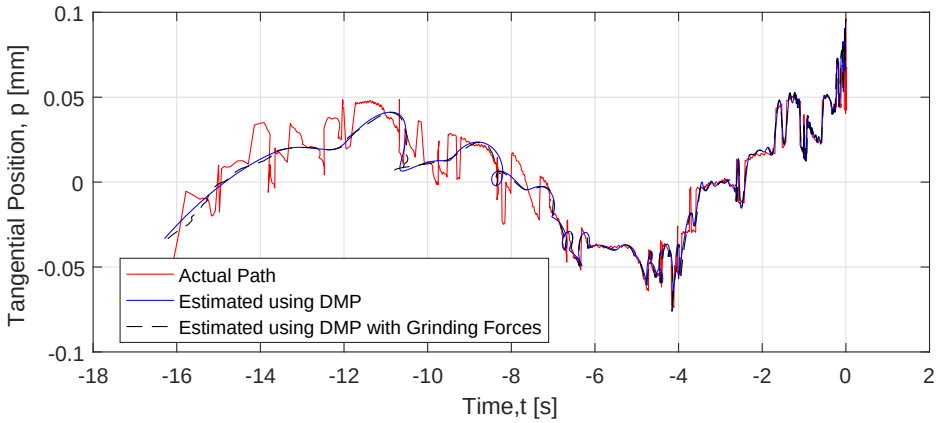

Figure 5.3: Experimental and estimated trajectories in 2 dimensions using DMP and DMP with deburring force

5.4 Conclusion

Human expert performs perfect deburring process using his/her set of motor capabilities and senses. The expert internally develops an interaction model by experience in his/her mind. This model adapts to changing environment accordingly due to expert's immense neural network. Instead of developing an explicit interaction model for deburring; the idea of utilizing a human expert's already developed internal model to generate trajectories of a robot for deburring operation is the core of this study. This is accomplished by the extended additional term of the modified Dynamic Movement Primitives (DMP) model. The nonlinear functions obtained from subjects, correspond to an expert's internal model of interaction and trained by a neural network.

CHAPTER 6

EXPERIMENTAL PROCEDURE

The aim of this thesis is to reduce the form error of a ground workpiece on a robotic grinding setup. As explained in chapter 3, DMP method is utilized to eliminate the form error on the workpiece due to tool deflections. For this purpose, three sets of experiments are designed and conducted.

First set of experiments is conducted to extract the non-linear function, f_{grind} given in (3.16). For this purpose, standard process is applied on a workpiece while forces on the spindle are recorded. Then, surface is measured in order to determine the amount of material remaining due to tool deflection.

Second set of experiments aims to validate that using DMP method form error can be reduced significantly compared to standard grinding with a non-stiff robotic setup by only changing depth of cut. Therefore, (3.19) is applied only to the translational motion in normal direction of the grinding process.

Lastly, form error can still occur due to the angular deviations of the tool tip. In order to eliminate this, third set of experiments is conducted by applying (3.19) to both the translational motion in normal direction and rotation about the tangential direction.

6.1 Force Relations Determination

In this section extraction of. The nonlinear function will be trained based on measured deflection and force values. The flow chart for the procedure is shown in Figure 6.1. First, a ramp is machined to the workpiece with specified initial height, h_1 and final height, h_2 on the robotic grinding setup. Then, this workpiece is machined to get a

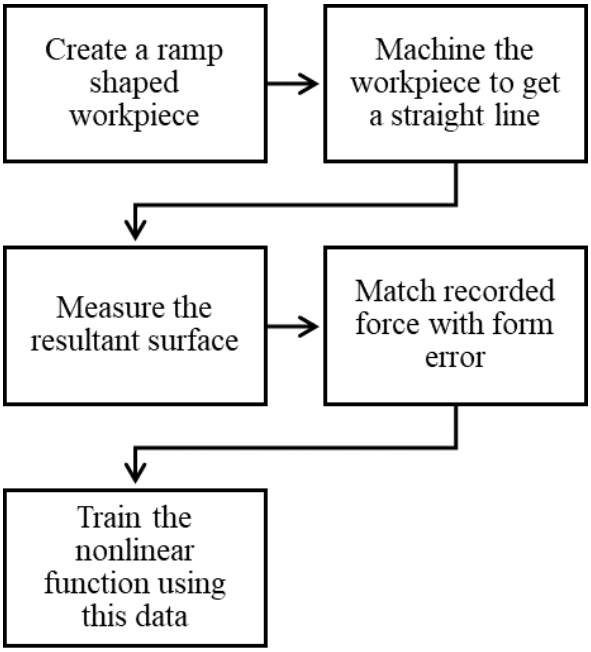

Figure 6.1: General flow scheme of the experiments

straight and flat surface by assigning the robot to move on a straight line as illustrated in Figure 6.2.The grinding forces are recorded during the process in the following form.

$$F = f(y) \tag{6.1}$$

The result of the process will not be as desired since the grinding forces cause tool deflection. The resultant surface is measured by the point laser scanner and the form error values are obtained in the following form.

$$\delta = f(x, y) \tag{6.2}$$

Also, rotation of the tool about the tangential direction is calculated by simply fitting lines on the measurements of the machined surface of the workpiece, Figure 6.4. Then, angular deviations are obtained in the following form.

$$\theta = f(y) \tag{6.3}$$

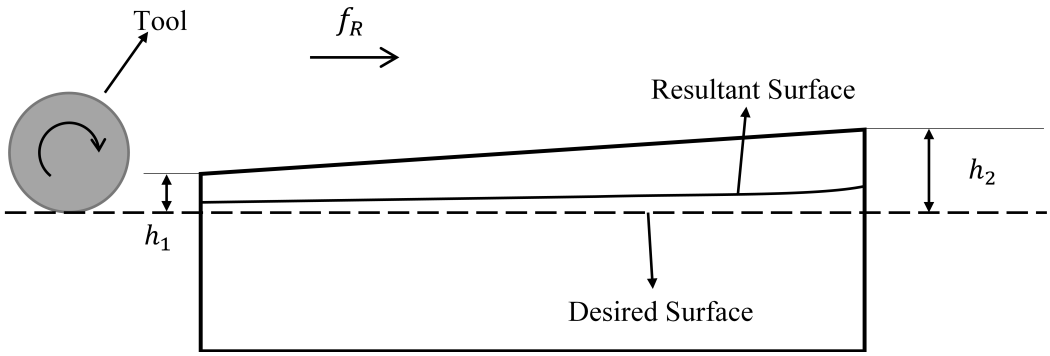

Figure 6.2: Illustration of the first set of experiments.

As a result, required data to train the nonlinear function is obtained by matching data of F and δ for equal y values and matching data of F and θ for equal y values, so (3.17) and (3.18) are obtained. Then, the nonlinear function, $f_{grind}(F_n, F_t)$ is trained by adjusting weights of the function to fit the function to the data.

6.1.1 Scanning Machined Surfaces

Scanning of the workpiece is used to determine the 3D surface profile of the pre-machined and machined workpieces. In this study, a certain rectangular shaped surface is machined, however, in order to measure it, its orientation is need to be determined. For this purpose, four points at the edges of the rectangular surface are need to be determined and then using these points a path for the surface scan can be generated. In Figure 6.3, the workpiece and the four points (r_1, r_2, r_3 and r_4) at the edges are illustrated.

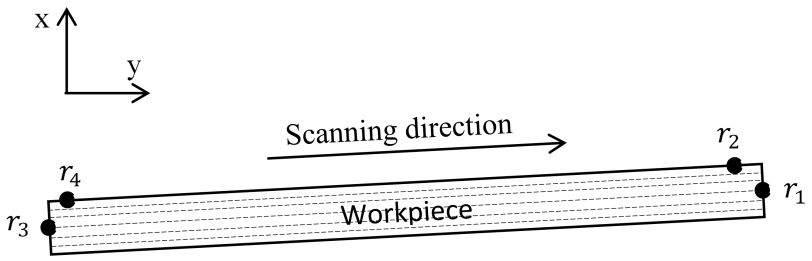

Figure 6.3: Illustration of the workpiece on the table of the robot with points at the edges.

The scanning direction is the direction of the vector connecting r_4 to r_2. Then the scanner follows multiple parallel lines in the scanning direction which are drawn with dashed lines in the Figure 6.3. End points of the lines are determined using r_1 and r_3.

After the scan is finished, a point cloud is obtained that has the information of the scanned surface. Using those points, the form error of the workpiece is calculated as well as the angular deviation of the workpiece by fitting lines perpendicular to scanning direction. Fitted lines on a workpiece to calculate angular deviation are illustrated in Figure 6.4.

6.2 Linear Deflection Compensation

After training the function in (3.17), DMP method is implemented for deflection compensation in normal direction. For this purpose, (3.17) is reduced to the following form.

$$\tau\dot{z} = \alpha_z(g - z) + f_{grind}(F_n) \tag{6.4}$$

Here, since the aim is to preserve a constant depth of cut, $f(x)$ is dropped. Also, since it does not effect the deflection in normal direction, tangential force, F_t, is eliminated from arguments of nonlinear function, f_{grind}.

6.2.1 Determination of DMP Parameters

In (6.4) there are two parameters, which are τ and α_z. These parameters affect the dynamic characteristics of the system.

Among these parameters, α_z determines the steady state value of z, which is the position of the tool in normal direction. At steady state, value of $\dot{z}$ approaches to zero, therefore, from (6.4) expression for z comes as below.

$$z = g + \frac{f_{grind}(F_n)}{\alpha_z} \tag{6.5}$$

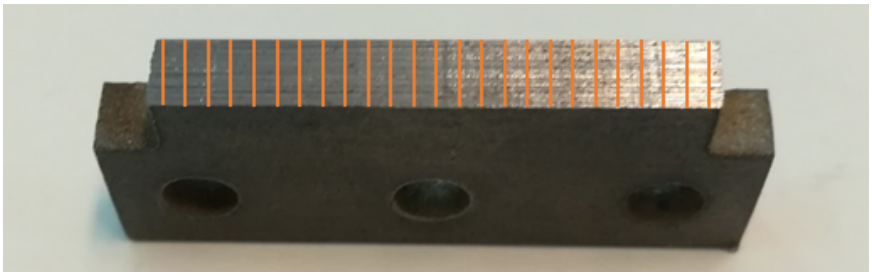

Figure 6.4: Fitted lines on a workpiece to calculate angular deviation.

By considering the above equation, it can be understood that the effect of nonlinear function $f_{grind}(F_n)$ on z is dependent to α_z. Increasing value of α_z results in smaller adjustments of the tool position while decreasing value of α_z increases the effect of $f_{grind}(F_n)$. Because $f_{grind}(F_n)$ gives estimate form error for a given F_n, setting $\alpha_z = 1$, assures achieving the desired surface at steady state.

Determination of τ depends on many parameters including spindle speed, feed rate and other tool and material properties. Since the trained nonlinear function is only applicable on unique tool and material pair and also for a specified tool length, data from the first set of experiments could be useful to settle the value of τ. Feeding F_n from those experiments to (6.4) for different τ values, it generates various trajectories. Comparing generated $(g - z)$ values with previously measured δ values, three fitting conditions can be observed. For τ getting larger values, $\dot{z}$ gets smaller so system becomes bulky and cannot respond to force changes in time. For τ getting smaller values, $\dot{z}$ gets larger and this causes a very responsive system which fits to even noisy fluctuations in the force data.

6.2.2 Machining Different Workpiece Profiles

There are four surface profiles machined to get a flat surface for validating that DMP method is working well to reduce form error significantly. These profiles are named as straight, ramped, trapezoidal and sinusoidal profiles, Figure 6.5.

Firstly, a straight profile is aimed to machined by constant material removal through the profile. For this profile, it is expected that force values remain almost constant since any grinding parameter is subjected to change except slight changes in depth of

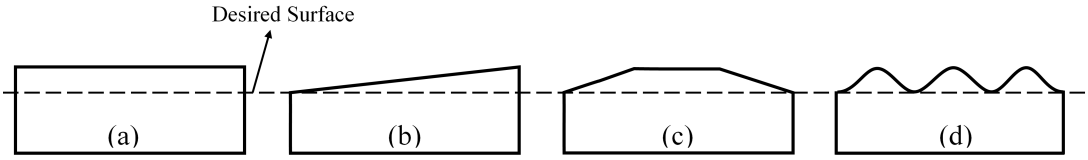

Figure 6.5: Different shapes of profiles. (a) Straight profile. (b) Ramped profile. (c) Trapezoidal profile. (d) Sinusoidal profile.

cut.

For the case of ramped profile, the depth of cut increases (or decreases) with the feed. By using this profile, response of the DMP system to the ramp input can be investigated.

The next one is the trapezoidal profile and it is a mixture of the first two profiles.

The last case of sinusoidal profile is used for observing the DMP system taking the force input from a wide range of values. This profile provides more dynamic environment compared to others. By changing the period and amplitude of the sinusoidal, its dynamic characteristic changes.

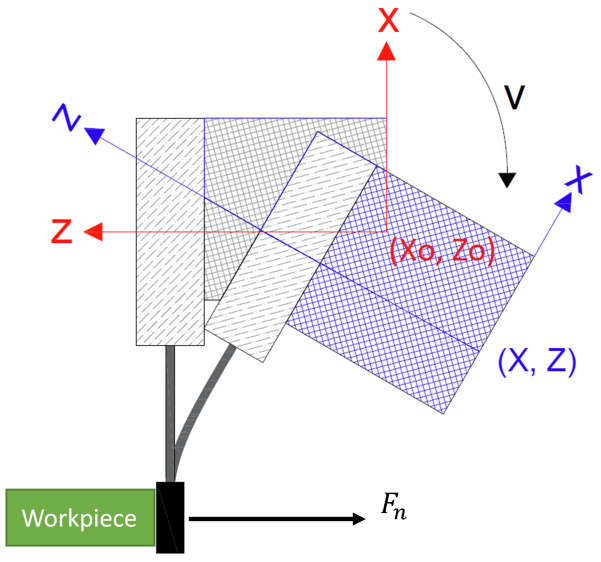

Figure 6.6: Two positions of the robot illustrating the angular deviation compansation action. (x_0, z_0) is the position of the robot for $v = 0$ and (x, z) is the position of the robot for a certain v value.

Each profile is machined twice. One of them is without using DMP so it is a standard grinding process. The other is using DMP for online trajectory generation using force input. Each profile is also measured with the laser scanner before and after the process. After measurements, mean, standard deviation and RMS values of the form error with respect to desired surface are calculated and compared.

6.3 Angular Deviation Compensation

The grinding forces cause also angular deviations on the tool tip as well as deflections. Therefore, linear deflection compensation should be extended to get more accurate surface finish with smaller form errors. Therefore, one more transformation system is added on top of the existing one to control the position of the tool.

$$\tau_v \dot{v} = \alpha_v(g_z - v) + f_{grind,v}(F_n) \tag{6.6}$$

Here, v is the rotational coordinate about the tangential direction (y-axis). Since tool is located at a distance from the origin of the robot, adding rotation to the system also results in translational motion at the tool. To eliminate this extra motion in x and z axes, extra terms should be added to these coordinates. Therefore, this positional adjustment of the robot is illustrated in Figure 6.6.

$$x = x_0 - d_x(1 - \cos(v)) - d_z \sin(v) \tag{6.7}$$

$$\tau_z \dot{z}_0 = \alpha_z(g_z - z_0) + f_{grind,z}(F_n) \tag{6.8}$$

$$z = z_0 - d_x \sin(v) + d_z(1 - \cos(v)) \tag{6.9}$$

Where, d_x and d_z are the offset of the tool tip from the origin of the robot in x and z axes. x_0 and z_0 are the coordinates of the robot with $v = 0$ (See. Figure 6.6). (6.8) is the same equation as (6.4) but the output is updated by additional terms.

Now, the system is available for angular deviation compensation as well as linear deflection compensation. The upcoming procedure is similar to section 6.2. Firstly, DMP parameters are determined using the method explained in section 6.2.1, in this case there are four of them.

Then, after determining DMP parameters, everything is ready to apply these equation to the grinding process. The method is again tested on the profiles shown in Figure 6.5. Each profile is measured with the laser scanner before and after the process. After measurements, mean, standard deviation and RMS values of the form error with respect to desired surface are calculated and compared with the results obtained by the linear deflection compensation method explained in section 6.2.

CHAPTER 7

RESULTS AND DISCUSSION

In this chapter, the results of the experiments explained in chapter 6 are presented and evaluated compared to standard robotic grinding (RG) process. Robotic grinding with DMP (RG-DMP) is also compared with robotic grinding process with PID (RG-PID) and ADRC (RG-ADRC) controllers. The criteria for the comparison is the flatness of the surface and also the form errors from the desired surface.

7.1 Force Relations Determination

As described in section 6.1, multiple workpieces are machined to obtain a flat surface. Then, from measured surface and recorded data, training data is created by matching them. Finally, $f_{grind,z}$ and $f_{grind,v}$ in (6.4) and (6.6) are trained with the training data. In Figures 7.1 and 7.2 , the training data and trained nonlinear functions linear deflection and angular deviation are presented.

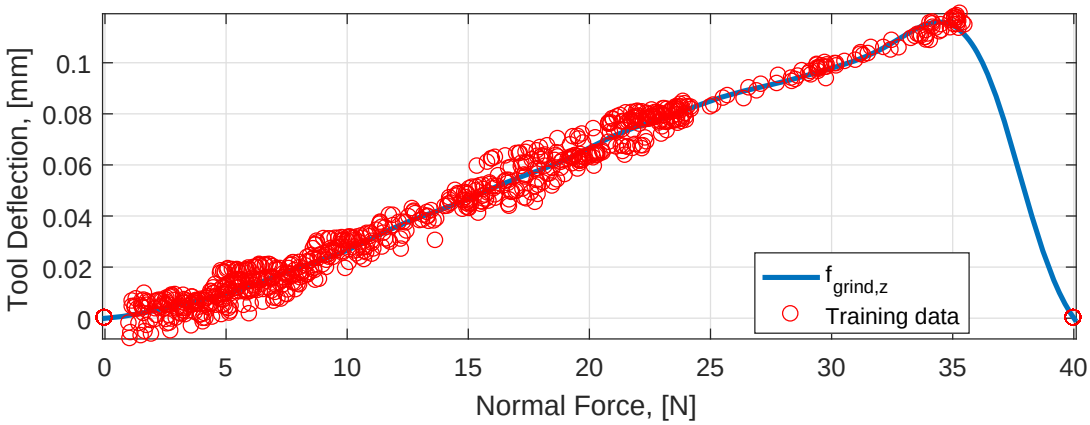

Figure 7.1: Training data and nonlinear function for linear deflection

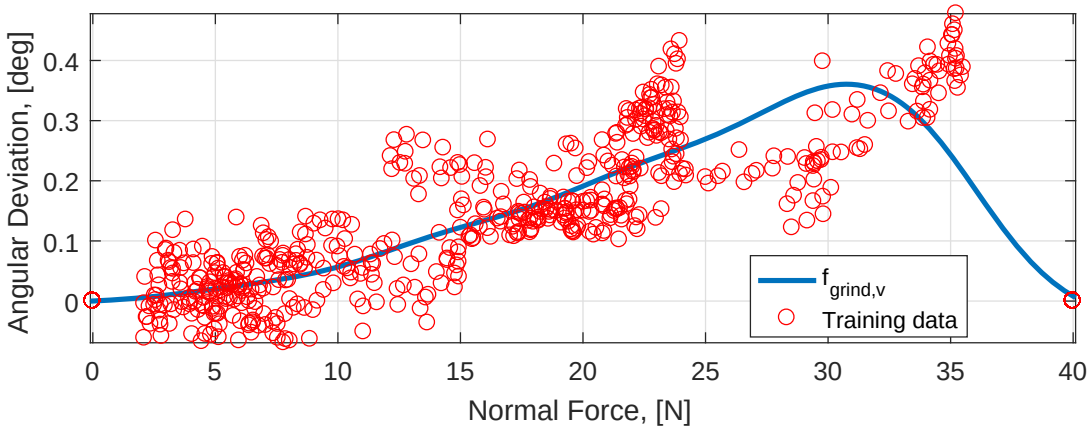

Figure 7.2: Training data and nonlinear function for angular deviation

In Figures 7.1 and 7.2, red scattered data is the training data obtained from experiments. For normal force values of 0 and $40\ N$, deflection and deviation is assigned to be 0 as well. Since tool goes more into the workpiece with the increasing normal force, this results in way more grinding forces so it could damage the tool and the setup. To avoid this, tool won't go into workpiece and keep force values lower than $40\ N$. The blue solid lines in the figures are the trained nonlinear functions that are used in DMP equations (6.4) and (6.6). Finally, using DMP equations with the nonlinear functions, deflections of the tool can be estimated and compensated.

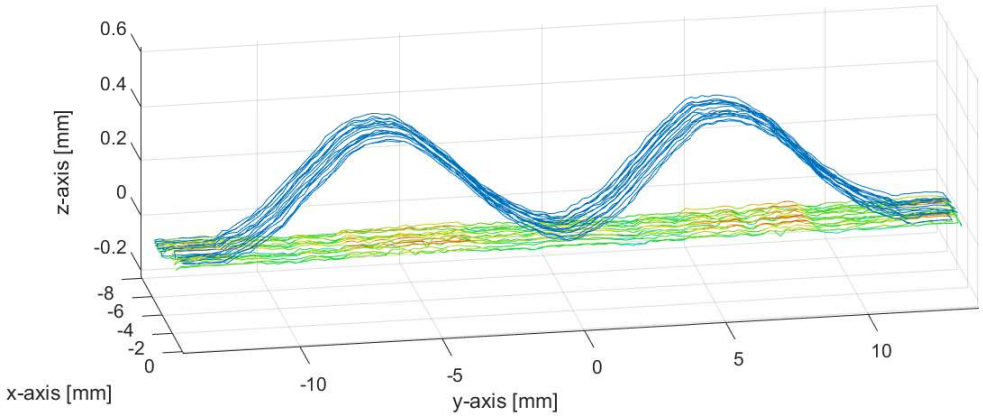

Figure 7.3: Surface scan of a workpiece before and after the grinding operation.

7.2 Linear Deflection and Angular Deviation Compensation

In this section, the grinding process is applied on specified profiles of the workpieces. Each process is performed with and without using the proposed methods, namely, linear deflection compensation with DMP and angular deviation compensation with DMP on top of linear deflection compensation. In other words, workpieces are first machined with no trajectory adjustment and deflection compensation, then, they are machined by only applying linear deflection compensation. Finally, they are machined by applying both linear deflection and angular deviation compensation. Also, surface of each workpiece is scanned with laser measurement sensor before and after the process. An example scan of a ground workpiece is shown in Figure 7.3, where, blue lines are the measured surface before the operation and colored lines are the measured surface after the operation. The color is changes from blue to red with increasing z value. The coloring is made in order to make the figure more understandable.

Table 7.1: Statistical values of form error and surface angle for "Almost Flat Surface".

Almost Flat Surface					
Linear Error [mm]			Angular Error [^{o}]		
MEAN	STD	RMS	MEAN	STD	RMS
0.0000	0.0096	0.0096	0.0000	0.0172	0.0172

In Tables 7.2-7.6, statistical measures for 12 machined surfaces are listed. From Figure 7.4 to Figure 7.8 surface scans of these surfaces are presented. The first column has the names of the profiles which are shown in Figure 6.5. The next number gives the maximum depth of cut on that profile. Second and third columns give the types of error which are mean, standard deviation and RMS values of the form error (Linear Error) with respect to desired surface and mean, standard deviation and RMS values of the surface angle (Angular Error) with respect to desired surface angle. Finally, the remaining columns has the error values of three different processes applied. Where, (SGP) stands for standard grinding process, that is no deflection compensation, (DMP-L) for linear deflection compensation with DMP and (DMP-AL) for angular deviation compensation with DMP on top of linear deflection compensation.

Table 7.2: Statistical values of form error and surface angle of the experiments from workpieces of straight profile machined with standard grinding and the two proposed methods.

Profile	Error Type		SGP	DMP-L	DMP-AL
Straight 450 µm	Linear Error [mm]	MEAN	0.0701	0.0091	0.0043
		STD	0.0231	0.0122	0.0117
		RMS	0.0738	0.0152	0.0125
	Angular Error [^{o}]	MEAN	0.2005	0.2120	0.0344
		STD	0.1089	0.1375	0.0516
		RMS	0.2292	0.2521	0.0630

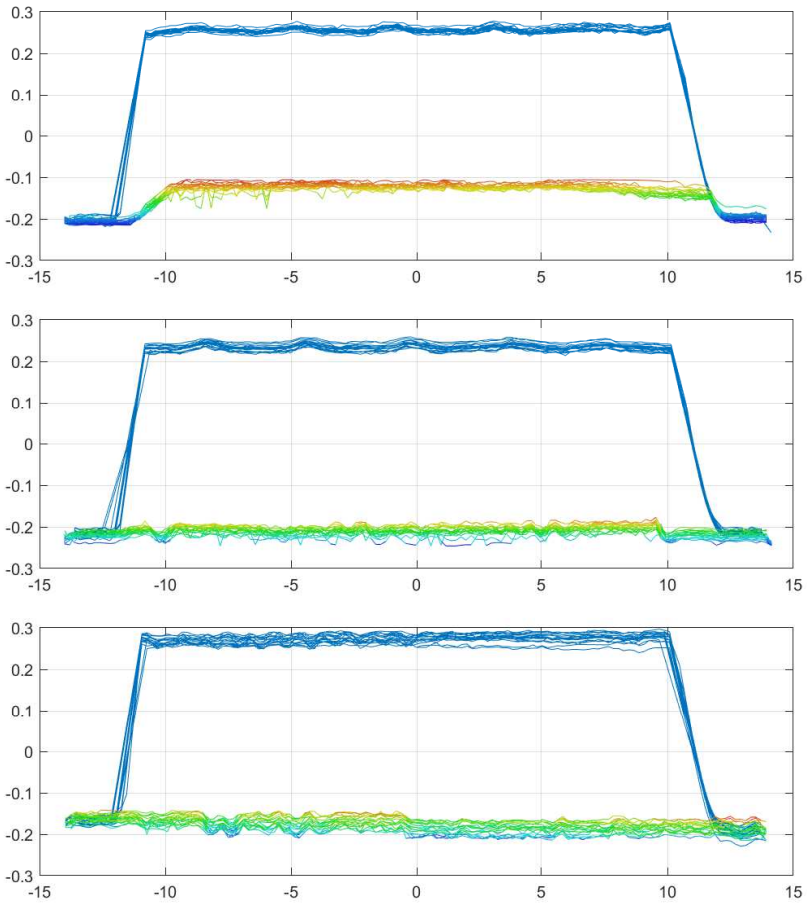

Figure 7.4: Results of grinding operations on Straight 450 µm. Y-Z view of scan. Top: SGP, Middle: DMP-L, Bottom: DMP-AL.

Table 7.3: Statistical values of form error and surface angle of the experiments from workpieces of ramped profile machined with standard grinding and the two proposed methods.

Profile	Error Type		SGP	DMP-L	DMP-AL
Ramped 450 µm	Linear Error [mm]	MEAN	0.0256	0.0037	0.0015
		STD	0.0180	0.0117	0.0137
		RMS	0.0313	0.0123	0.0138
	Angular Error [^{o}]	MEAN	0.1516	0.1776	0.0573
		STD	0.0802	0.0974	0.0516
		RMS	0.1675	0.2005	0.0745

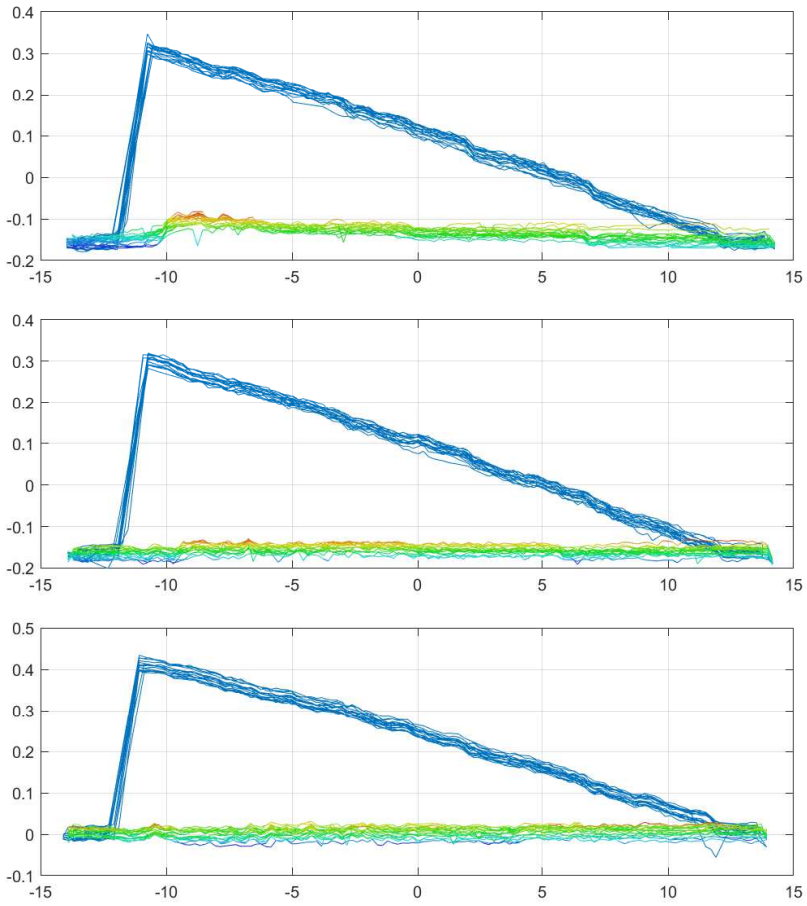

Figure 7.5: Results of grinding operations on Ramped 450 µm. Y-Z view of scan. Top: SGP, Middle: DMP-L, Bottom: DMP-AL.

Table 7.4: Statistical values of form error and surface angle of the experiments from workpieces of straight profile machined with standard grinding and the linear deflection compensation method.

Profile	Error Type		SGP	DMP-L
Straight 300 µm	Linear Error [mm]	MEAN	0.0139	0.0047
		STD	0.0116	0.0122
		RMS	0.0181	0.0131
	Angular Error [°]	MEAN	0.2349	0.0516
		STD	0.1203	0.0688
		RMS	0.2636	0.0859

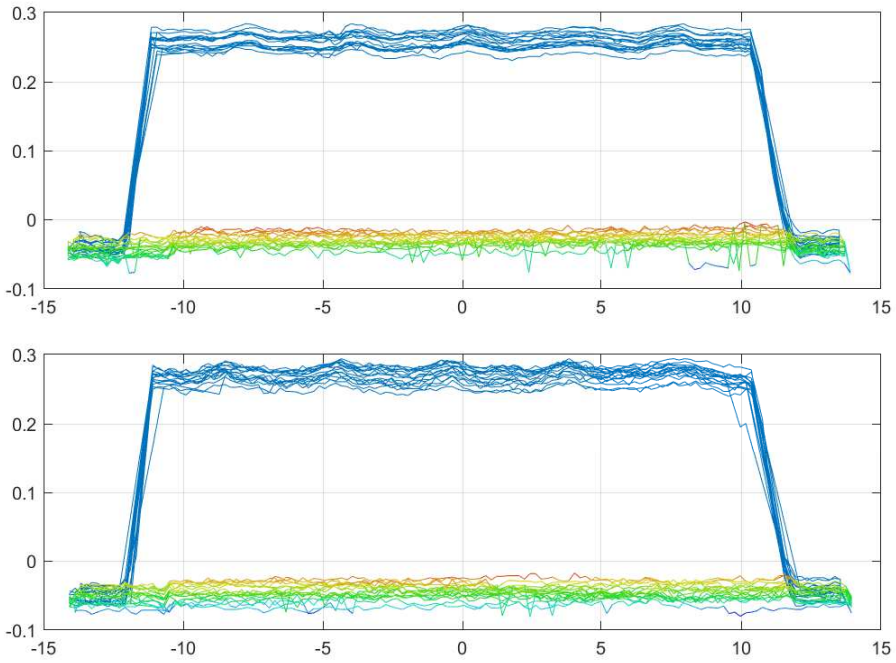

Figure 7.6: Results of grinding operations on Straight 300 µm. Y-Z view of scan. Top: SGP, Middle: DMP-L, Bottom: DMP-AL.

Table 7.5: Statistical values of form error and surface angle of the experiments from workpieces of trapezoidal profile machined with standard grinding and the linear deflection compensation method.

Profile	Error Type		SGP	DMP-L
Trapezoid 450 µm	Linear Error [mm]	MEAN	0.0319	0.0123
		STD	0.0207	0.0099
		RMS	0.0380	0.0158
	Angular Error [°]	MEAN	0.0458	0.0573
		STD	0.0401	0.0539
		RMS	0.0630	0.0802

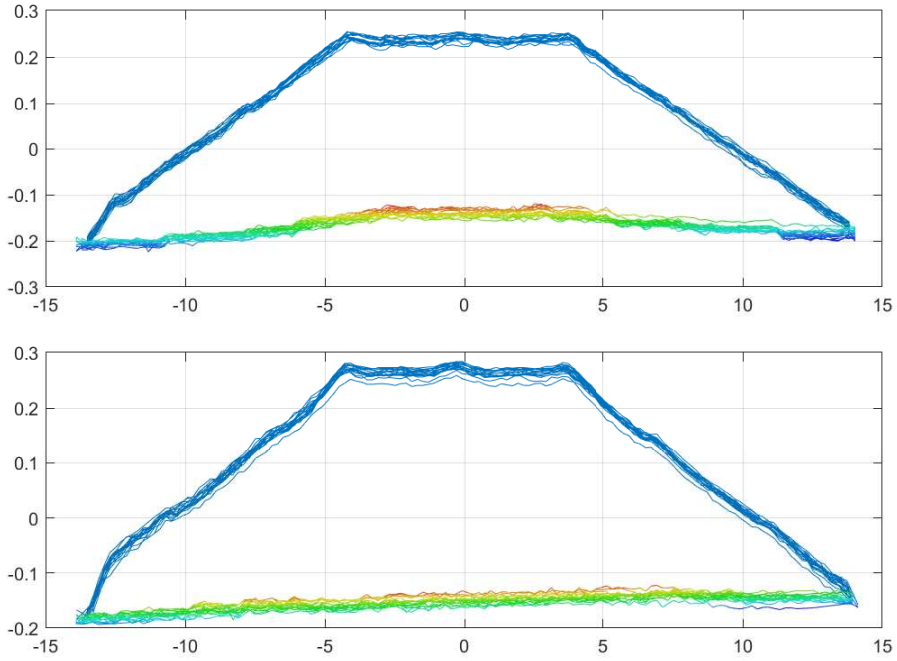

Figure 7.7: Results of grinding operations on Trapezoidal 450 µm. Y-Z view of scan. Top: SGP, Middle: DMP-L, Bottom: DMP-AL.

Table 7.6: Statistical values of form error and surface angle of the experiments from workpieces of sinusoidal profile machined with the two proposed methods.

Profile	Error Type		DMP-L	DMP-AL
Sinusoidal 400 µm	Linear Error [mm]	MEAN	0.0136	0.0033
		STD	0.0133	0.0088
		RMS	0.0190	0.0094
	Angular Error [^{o}]	MEAN	0.1057	0.0516
		STD	0.1363	0.0458
		RMS	0.0859	0.0688

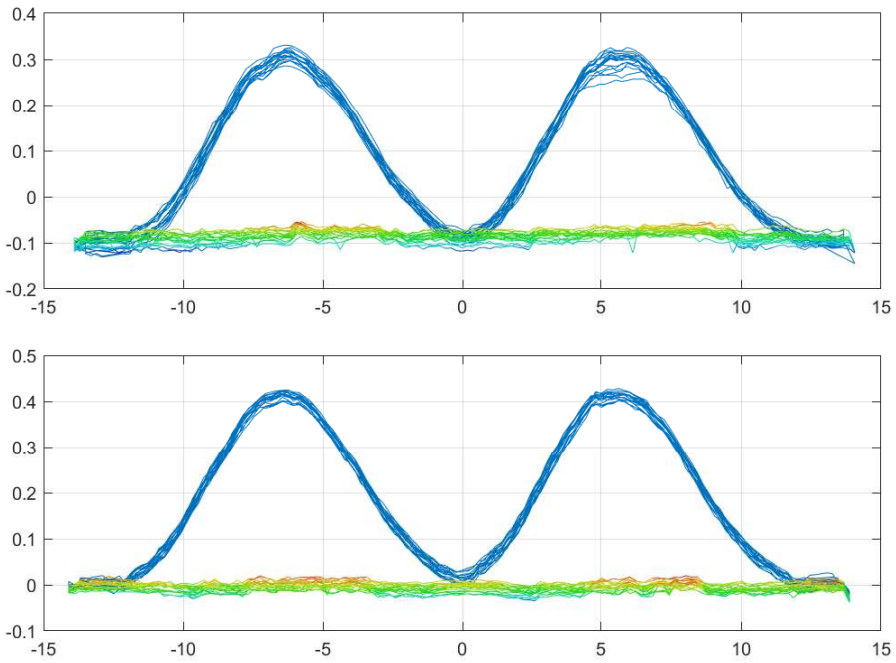

Figure 7.8: Results of grinding operations on Sinusoidal 400 µm. Y-Z view of scan. Top: SGP, Middle: DMP-L, Bottom: DMP-AL.

In Tables 7.2-7.6, mean values of linear and angular error is calculated by taking the average of errors of individual measurements from the reference surface, i.e. the almost flat surface. Then, the standard deviation values are calculated using the formula below.

$$STD = \sqrt{\frac{\sum_{i=1}^{n}(e_i - \mu_e)^2}{n}} \tag{7.1}$$

Also, RMS values are calculated by the following formula.

$$RMS = \sqrt{\frac{\sum_{i=1}^{n}(e_i)^2}{n}} \tag{7.2}$$

When these statistical values are investigated, it can be seen that linear deflection mean values are highest for standard process, then, linear deflection compensation comes and finally, angular deviation compensation method has the lowest average form error. However, to determine the surface quality, standard deviation and RMS values of the form errors are calculated and tabulated. Here, standard deviation can be treated as a measure for the deviations in the form error of the surface. Therefore, resultant surface roughness and the quality of the processes can be compared among these values. For standard deviation values, results from DMP method used are generally better than the ones from standard grinding. Still, for Straight 300 µm (SGP) has very similar standard deviation with Straight 300 µm DMP-L. This could be because of the low grinding forces which pushes the differences in the methods into the background. DMP-AL provides average of 63% less mean of linear error but only 7% less standard deviation of linear error than DMP-L. As a result, DMP-AL does not manage to have distinctively better standard deviation, and surface quality compared to DMP-L.

For the error of angular deviation, DMP-AL shows its eligibility and has significantly lower mean of angular error with respect to other two processes, SGP and DMP-L. Also, from standard deviation respect, DMP-AL has lower values with respect to other two processes, SGP and DMP-L. DMP-AL provides average of 67% less mean of angular error and 49% less angular error deviation than DMP-L.

In Table 7.1, the least error values of the surface achievable with the grinding setup is presented. This one named as "Almost Flat Surface" because, unlike other experiments, the workpiece is machined for many passes to obtain best possible surface achievable with the setup. Therefore, results for "Almost Flat Surface" are the perfect results if everything goes ideally. When, this least error values are compared with the ones in Tables 7.2-7.6, it can be conclude that proposed methods could achieve standard deviation values of linear error at most 40% higher than the least standard deviation values of linear error. However, the standard deviation values of angular error are at least 160% higher than the least standard deviation values of angular error.

7.3 Tool Deflection Compensation with PID and ADRC

In his work [5], Donder presented a method to compensate the form shaping errors in grinding operations due to the lack of a prior knowledge of the surface profile. In his study, the tool deflections are computed from the grinding forces in real time and the compensation is performed by the hexapod robot in 6-DoF and two different control algorithms namely PID control and Active Disturbance Rejection Control were tested on a robotic grinding setup and the experiment results are discussed. From this work, RMS values of form resulting from PID controller with different reference normal forces and ADRC are presented in Table 7.7. Also, the angle of the surface form resulting from PID controller with different reference normal forces and ADRC presented in Table 7.8.

Table 7.7: RMS values of form resulting from PID controller with different reference normal forces and ADRC.

	PID ($F_n = 7.5$N)	PID ($F_n = 10$N)	ADRC ($F_n = 7.5$N)
RMS [mm]	0.042	0.060	0.065

By comparing the error results of linear deflection of grinding process with DMP (Tables 7.2-7.6) and PID and ADRC (Table 7.7), it can be conclude that grinding process with DMP has at least 55% lower RMS value with respect to PID control and at least 71% lower RMS value with respect to ADRC. Then, by comparing the

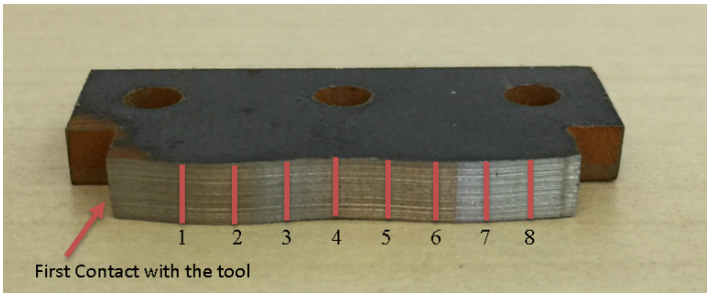

Figure 7.9: Ground workpiece with the lines that the angle of the surface form is measured.

Table 7.8: The angle of the surface form resulting from PID controller with different reference normal forces and ADRC. All values are with unit [^{o}].

Numbered lines in Figure 7.9	1	2	3	4	5	6	7	8	Mean	STD
PID $F_n = 7.5$N	-0.15	-0.17	-0.12	-0.14	-0.10	-0.06	-0.09	-0.12	-0.119	0.035
PID $F_n = 10$N	-0.16	-0.12	-0.13	-0.11	-0.05	-0.09	-0.09	-0.10	-0.106	0.032
ADRC $F_n = 7.5$N	-0.19	-0.16	-0.13	-0.11	-0.12	-0.09	-0.13	-0.12	-0.131	0.031

error results of angular deviation of grinding process with DMP (Tables 7.2-7.6) and PID and ADRC (Table 7.8), it can be said that grinding process with DMP has at least 28% higher STD value with respect to PID control and at least 45% higher STD value with respect to ADRC. Note that, PID and ADRC are applied to keep the force at a certain level and these 7.5N and 10N forces are small forces compared to the forces encountered for example during machining a Straight 450 µm profile with DMP which has average force of 24.67N.

CHAPTER 8

CONCLUSION AND FUTURE WORK

8.1 Conclusion

In this thesis study, DMP method is utilized for trajectory generation of robotic grinding operation. In standard robotic deburring, interaction forces can cause significant deflection on the tool, workpiece and the robotic system. As a result, form errors occur. Using force data as perception and form error as position, DMP method is trained and used to predict deflection on the tool and make adjustments on the trajectory, while performing the deburring operation online. Four different surface profiles (Straight, Ramped, Trapezoidal and Sinusoidal) machined to get a flat surface.

The results of robotic deburring process with DMP (RD-DMP) show that, by performing linear and angular adjustments, the form errors on the machined workpieces decreased significantly compared to standard deburring (RD). It was shown that the average form error of the surface profile obtained by RD-DMP is roughly 80% less than the surface profile obtained by RD. Also, the average angular error of the surface profile obtained by RD-DMP is roughly 70% less than angular error of the surface obtained by RD. This result validates that DMP method is working pretty well to decrease the form error considerably.

In addition, the DMP method for angular deviation and linear deflection compensation (DMP-AL) and the DMP method for linear deflection compensation (DMP-L) are also compared. DMP-AL provides average of 63% less average linear error but only 7% less standard deviation of linear error than DMP-L. Also, DMP-AL provides average of 67% less average angular error and 49% less angular error deviation than DMP-L.

Moreover, RD-DMP is also compared with robotic deburring process with PID (RD-PID) and ADRC (RD-ADRC) controllers. The form error of the surface profile obtained by RD-DMP is roughly 28% higher than the surface profile obtained by RD-PID and 45% times higher than RD-ADRC. Also, based on literature survey on the same deburring robot, PID method result is better than ADRC in this application.

8.2 Future Work

In this work, DMP is utilized on two axes of a 6-DoF robotic deburring robot. The first extension of this work can be increasing the number of axes controlled by DMP. By this extension, the process can easily be used for grinding on very complex workpieces and surfaces like propeller, airfoil shape of the wing, etc. as long as the location of the part is known and the machine code is generated for machining.

Another improvement can be made by using nonlinear functions with more complex structures. In this study only forces are taken into account, however, overall stiffness of the system can be trained on a function for all positions and configurations of the robotic system.

REFERENCES

[1] K. Acikgoz, P. Parvizi, A. Donder, M. C. Ugurlu, and E. b. Konukseven. Dynamic movement primitives and force feedback: Teleoperation in precision grinding process. In *Electrical and Electronics Engineering (ELECO), 2017 10th International Conference on*, pages 722–726, 2017.

[2] A. Alissandrakis, C. L. Nehaniv, and K. Dautenhahn. Imitation with ALICE: Learning to imitate corresponding actions across dissimilar embodiments. *IEEE Transactions on Systems, Man, and Cybernetics-Part A: Systems and Humans*, 32(4):482–496, 2002.

[3] C. Breazeal and B. Scassellati. Robots that imitate humans. *Trends in cognitive sciences*, 6(11):481–487, 2002.

[4] S. Calinon and A. Billard. Incremental learning of gestures by imitation in a humanoid robot. In *Proceedings of the ACM/IEEE international conference on Human-robot interaction*, pages 255–262, 2007.

[5] A. Donder. *Active compliance control structure design for a robotic-grinding machine*. Master's thesis, Middle East Technical University, Department of Mechanical Engineering, 2017.

[6] L. K. Gillespie. Deburring, deflashing, and edge finishing of microparts. In *Technical Paper - Society of Manufacturing Engineers*, 2010.

[7] G. M. Hayes and J. Demiris. *A robot controller using learning by imitation*. University of Edinburgh, Department of Artificial Intelligence, 1994.

[8] N. Hogan and D. Sternad. Dynamic primitives of motor behavior. *Biological Cybernetics*, 106(11-12):727–739, 2012.

[9] A. J. Ijspeert, J. Nakanishi, H. Hoffmann, P. Pastor, and S. Schaal. Dynamical movement primitives: learning attractor models for motor behaviors. *Neural computation*, 25(2):328–73, 2013.

[10] H. Kazerooni, J. J. Bausch, and B. M. Kramer. An Approach to Automated Deburring by Robot Manipulators. *Journal of Dynamic Systems, Measurement, and Control*, 108(4):354, 1986.

[11] C. T. Kim and J. J. Lee. Training two-layered feedforward networks with variable projection method. *IEEE Transactions on Neural Networks*, 2008.

[12] J. Kober, M. Gienger, and J. J. Steil. Learning Movement Primitives for Force Interaction Tasks. In *Proceedings - IEEE International Conference on Robotics and Automation*, volume 3, pages 3192–3199, 2015.

[13] Y. Kuniyoshi, M. Inaba, and H. Inoue. Learning by watching: Extracting reusable task knowledge from visual observation of human performance. *IEEE transactions on robotics and automation*, 10(6):799–822, 1994.

[14] M. Latifinavid, A. Donder, and E. ilhan Konukseven. High-performance parallel hexapod-robotic light abrasive grinding using real-time tool deflection compensation and constant resultant force control. *International Journal of Advanced Manufacturing Technology*, 96(9-12):3403–3416, 2018.

[15] L. Liao, F. J. Xi, and K. Liu. Modeling and control of automated polishing/deburring process using a dual-purpose compliant toolhead. *International Journal of Machine Tools and Manufacture*, 48(12-13):1454–1463, 2008.

[16] S. Liu, H. Asada, and A. Control. Adaptive Control of Deburring Robots Based on Human Skill Models. *Decision and Control, 1991., Proceedings of the 30th IEEE Conference on*, (December):348–353, 1991.

[17] S. Niekum, S. Osentoski, G. Konidaris, and A. G. Barto. Learning and generalization of complex tasks from unstructured demonstrations. In *Intelligent Robots and Systems (IROS), 2012 IEEE/RSJ International Conference on*, pages 5239–5246, 2012.

[18] A. Paraschos, C. Daniel, J. R. Peters, and G. Neumann. Probabilistic movement primitives. In *Advances in neural information processing systems*, pages 2616–2624, 2013.

[19] P. Parvizi, M. Ugurlu, K. Acikgoz, and E. Konukseven. Parametrization of robotic deburring process with motor skills from motion primitives of human

skill model. In *2017 22nd International Conference on Methods and Models in Automation and Robotics, MMAR 2017*, 2017.

[20] P. Pastor, H. Hoffmann, T. Asfour, and S. Schaal. Learning and Generalization of Motor Skills by Learning from Demonstration. *Proceedings of the 2009 IEEE International Conference on Robotics and Automation*, pages 1293–1298, 2009.

[21] B. E. Perk and J.-J. E. Slotine. Motion primitives for robotic flight control. *arXiv preprint cs/0609140*, 2006.

[22] S. Schaal. Is imitation learning the route to humanoid robots? *Trends in cognitive sciences*, 3(6):233–242, 1999.

[23] S. Schaal. Dynamic Movement Primitives – A Framework for Motor Control in Humans and Humanoid Robotics. *Adaptive Motion of Animals and Machines*, (1):261–280, 2006.

[24] S. Schaal, A. Ijspeert, and A. Billard. Computational approaches to motor learning by imitation. *Philosophical transactions of the Royal Society of London. Series B, Biological sciences*, 358(1431):537–47, 2003.

[25] S. Schaal, P. Mohajerian, and A. Ijspeert. Dynamics systems vs. optimal control - a unifying view, 2007.

[26] M. Schneider and W. Ertel. Robot Learning by Demonstration with local Gaussian process regression. In *IROS*, pages 255–260, 2010.

[27] K. G. Sheela and S. N. Deepa. Review on methods to fix number of hidden neurons in neural networks. *Mathematical Problems in Engineering*, 2013.